

AD A140025

RADC-TR-83-261, Vol I (of two)
Interim Report
December 1983



ACROSS ELEVEN (ACTIVE CONTROL OF SPACE STRUCTURES)

The Charles Stark Draper Laboratory, Inc.

Sponsored by
Defense Advanced Research Projects Agency (DOD)
ARPA Order No. 3655

APPROVED FOR PUBLIC RELEASE; DISTRIBUTION UNLIMITED

The views and conclusions contained in this document are those of the authors and should not be interpreted as necessarily representing the official policies, either expressed or implied, of the Defense Advanced Research Projects Agency or the U.S. Government.

DTIC FILE COPY

ROME AIR DEVELOPMENT CENTER
Air Force Systems Command
Griffiss Air Force Base, NY 13441

DTIC
ELECTE
S **D**
APR 11 1984

D

84 04 11 004

This report has been reviewed by the RADC Public Affairs Office (PA) and is releasable to the National Technical Information Service (NTIS). At NTIS it will be releasable to the general public, including foreign nations.

RADC-TR-83-261, Vol I (of two) has been reviewed and is approved for publication.

APPROVED:



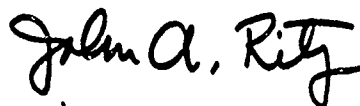
RICHARD W. CARMAN
Project Engineer

APPROVED:



FRANK J. REHM
Technical Director
Surveillance Division

FOR THE COMMANDER:



JOHN A. RITZ
Acting Chief, Plans Office

If your address has changed or if you wish to be removed from the RADC mailing list, or if the addressee is no longer employed by your organization, please notify RADC (OCSE) Griffiss AFB NY 13441. This will assist us in maintaining a current mailing list.

Do not return copies of this report unless contractual obligations or notices on a specific document requires that it be returned.

Accession For	
NTIS GRA&I	<input checked="" type="checkbox"/>
DTIC TAB	<input type="checkbox"/>
Unannounced	<input type="checkbox"/>
Justification	
By	
Distribution/	
Availability Codes	
Dist	Avail and/or Special
A/1	



ACOSS ELEVEN (ACTIVE CONTROL OF SPACE STRUCTURES)
Vol I

Thomas H. Brooks
Virendran Mahajan
Daniel R. Hegg

Glen J. Kissel
Harris N. McClamroch
James D. Turner

"Original contains color
plates. All DTIC reproductions
will be in black and
white."

Contractor: The Charles Stark Draper Laboratory, Inc.
 Contract Number: F30602-81-C-0180
 Effective Date of Contract: 27 April 1981
 Contract Expiration Date: 27 April 1984
 Short Title of Work: ACOSS Eleven (Active Control of Space Structures)

Program Code Number: 1E20
 Period of Work Covered: Nov 82 - May 83

Principal Investigator: Dr. Keto Soosaar
 Phone: (617) 258-2575

Project Engineer: Richard W. Carman
 Phone: (315) 330-3148

Approved for public release; distribution unlimited

This research was supported by the Defense Advanced Research
 Projects Agency of the Department of Defense and was monitored
 by Richard W. Carman (OCSE), Griffiss AFB NY 13441, under
 Contract F30602-81-C-0180.

UNCLASSIFIED

SECURITY CLASSIFICATION OF THIS PAGE (When Data Entered)

REPORT DOCUMENTATION PAGE		READ INSTRUCTIONS BEFORE COMPLETING FORM
1. REPORT NUMBER RADC-TR-83-261, Vol 1 (of two)	2. GOVT ACCESSION NO. AD-A10025	3. RECIPIENT'S CATALOG NUMBER
4. TITLE (and Subtitle) ACOSS ELEVEN (ACTIVE CONTROL OF SPACE STRUCTURES)		5. TYPE OF REPORT & PERIOD COVERED Interim Report Nov 82 - May 83
		6. PERFORMING ORG. REPORT NUMBER CSDL-R-1648
7. AUTHOR(s) Thomas H. Brooks Glen J. Kissel Virendran Mahajan Harris N. McClanahan Daniel R. Hegg James D. Turner		8. CONTRACT OR GRANT NUMBER(s) F30602-81-C-0180
9. PERFORMING ORGANIZATION NAME AND ADDRESS The Charles Stark Draper Laboratory, Inc. 555 Technology Square Cambridge MA 02139		10. PROGRAM ELEMENT, PROJECT, TASK AREA & WORK UNIT NUMBERS 62301E C6550104
11. CONTROLLING OFFICE NAME AND ADDRESS Defense Advanced Research Projects Agency 1400 Wilson Blvd Arlington VA 22209		12. REPORT DATE December 1983
14. MONITORING AGENCY NAME & ADDRESS (if different from Controlling Office) Rome Air Development Center (OCSE) Griffiss AFB NY 13441		13. NUMBER OF PAGES 64
		15. SECURITY CLASS. (of this report) UNCLASSIFIED
		15a. DECLASSIFICATION/DOWNGRADING SCHEDULE N/A
16. DISTRIBUTION STATEMENT (of this Report) Approved for public release; distribution unlimited		
17. DISTRIBUTION STATEMENT (of the abstract entered in Block 20, if different from Report) Same		
18. SUPPLEMENTARY NOTES RADC Project Engineer: Richard W. Carman (OCSE)		
19. KEY WORDS (Continue on reverse side if necessary and identify by block number) Draper Integrated Simulations Deconvolution Space-Based IR Surveillance Systems Active Mirrors Infrared Terrestrial Scene Simulation Mirror Deformations Line-of-Sight Stabilization Wavefront Errors Clutter Leakage Ray Tracing		
20. ABSTRACT (Continue on reverse side if necessary and identify by block number) Simulation Extension: The overall objective of the Simulation Extensions project is to identify and quantify those generic mission, scenario and sensor parameters (as well as their interactions) which drive the performance of space-based staring IR surveillance systems. The approach taken to achieve this overall objective has proceeded along two main avenues: Simulation Enhancements, and Simulation Applications. Efforts in the Simulation Enhancements area are directed toward generali-		

UNCLASSIFIED

SECURITY CLASSIFICATION OF THIS PAGE (When Data Entered)

UNCLASSIFIED

SECURITY CLASSIFICATION OF THIS PAGE (When Data Entered)

cont. zing those models in the Draper Integrated Simulations (DIS) which are too limited in scope or perhaps restricted to one particular system. In support of the Simulation Enhancements effort, work has been performed (or is in progress) on models for the platform, sensor (including focal plane and signal processor), and scene. The status of these efforts is summarized.

Utilizing the tools developed as a result of the Simulation Enhancements work, the Simulation Applications effort studies issues related to generic surveillance system performance drivers. Results are reported from a study which examines the effects of spectral band selection and scene local time of day on line-of-sight jitter-induced clutter leakage through the signal processor of a generic surveillance system.

Halo Optics: CSDL prepared a deconvolution test to validate Itek's deconvolution algorithm for correcting a deformed HALO optical system. The algorithm uses the wavefront errors measured by a wavefront sensor to determine the actuator signals. This report describes a limited blind test and concludes that the algorithm successfully determined the actuator displacements from the wavefront errors provided in this test. Recommendations for a more complete test are outlined.

UNCLASSIFIED

SECURITY CLASSIFICATION OF THIS PAGE (When Data Entered)

TABLE OF CONTENTS

<u>Section</u>	<u>Page</u>
1 INTRODUCTION.....	1
1.1 Simulation Extensions.....	1
1.2 HALO Optics.....	1
2 SIMULATION EXTENSIONS PROJECT.....	3
2.1 Introduction.....	3
2.2 Simulation Enhancements.....	3
2.2.1 Platform Simulation.....	3
2.2.2 Sensor Simulation.....	5
2.2.3 Scene Simulation.....	5
2.3 Simulation Applications.....	6
2.4 Conclusions.....	17
3 HALO OPTICS/DECONVOLUTION TEST.....	19
3.1 Introduction.....	19
3.2 Optical System for Deconvolution Test.....	19
3.3 Actuator Distribution and Influence Function.....	19
3.4 Mirror Deformations.....	23
3.5 Selection of Point Objects.....	23
3.6 Mirror Footprints.....	23
3.7 Wavefront Errors.....	32
3.8 Test Results.....	32
3.8.1 Mirror Deformations.....	32
3.8.2 Wavefront Errors.....	39
3.8.3 Point-Spread Functions.....	39
3.9 Discussion, Conclusions and Recommendations.....	39
REFERENCES.....	43

ACKNOWLEDGEMENT

This report was prepared by The Charles Stark Draper Laboratory, Inc., under Contract F30602-81-C-0180 and documents progress for the reporting period of November 1982 through May 1983 on the Simulation Extensions Project and the HALO Optics program.

The Program Manager at CSDL is Dr. Keto Soosaar. The Project Manager for the Simulation Extensions Project is Mr. Thomas Brooks. Mr. Brooks was supported by Mr. Saul Serben, Ms. Lois Fink, Mr. Jacques Govignon, and Ms. Karen Swiech. The Project Manager and the principal investigator of the HALO Optics program is Dr. Virendra N. Mahajan. Dr. Mahajan was supported in his efforts by Mr. Jacques Govignon and Mr. Carl Heinzl.

Publication of this report does not constitute approval by the Defense Advanced Research Projects Agency or the United States Government of the findings or conclusions contained herein. It is published for the exchange and stimulation of ideas.

SECTION 1

INTRODUCTION

1.1 Simulation Extensions

The objective of this project is to identify and quantify those generic mission, scenario and sensor parameters (as well as their interactions) which drive the performance of space-based staring IR surveillance systems. These efforts have been divided into two efforts: Simulation Enhancements; and Simulation Applications.

Work in the Simulation Enhancements area is directed toward generalizing those models in the Draper Integrated Simulations (DIS) which are too limited in scope or perhaps restricted to one particular system. Models have been prepared for the platform, sensor (including focal plane and signal processor), scene, and techniques for interfacing the DIS with an in-house image processor for graphics display.

The Simulation Applications effort studies issues related to generic surveillance system performance drivers using tools from the Simulation Enhancement effort. Typical examples are sensor line-of-sight stability, focal D^* , and critical scene/scenario characteristics.

1.2 HALO Optics

HALO is a multi-mirror large optical imaging system with a wide field of view. To maintain alignment as well as image quality, the mirrors are actively controlled with actuators. The term "deconvolution" implies a sensing and control scheme by which a deformed HALO optical system is corrected in near real time. In one of the techniques worked on by the Itek Corporation, the wavefront errors of the deformed system are measured with a wavefront sensor for several object points near the edge of the field-of-view of the system. The wavefront sensor is placed around the focal plane. The wavefront errors are decomposed into mirror figure errors and actuator displacements are generated to correct them with a deconvolution algorithm. This report describes a limited blind test that CSDL prepared for Itek to test and validate this algorithm. We conclude that the algorithm successfully determined the actuator displacements from the wavefront errors considered in this test. The residual wavefront errors were negligibly small and below the wavefront sensor noise.

It is recommended that one more blind test be prepared for Itek's deconvolution algorithm to include more realism. Some of the desirable features of this test are listed below.

- 1) Mirror deformations will not be produced by the actuators used for correction, because, in practice, a mirror is not deformed by the movement of actuators.
- 2) Some static aberrations will be added to the optical system to simulate a nondiffraction-limited undeformed system.

- 3) The on-axis wavefront error data may not be excluded, since the wavefront sensor placed around the HALO focal plane cannot sense it.
- 4) The actuator influence functions used for mirror figure correction will be slightly different from those used by Itek in their algorithm, to simulate errors in the knowledge of influence function.
- 5) The influence function for edge actuators may be different from that for interior actuators.

SECTION 2

SIMULATION EXTENSIONS PROJECT

2.1 Introduction

The overall objective of this project is to identify and quantify those generic mission, scenario and sensor parameters (as well as their interactions) which drive the performance of space-based staring IR surveillance systems. The approach taken to achieve this overall objective has proceeded along two main avenues: Simulation Enhancements; and Simulation Applications.

Efforts in the Simulation Enhancements area are directed toward generalizing those models in the Draper Integrated Simulations (DIS) which are too limited in scope or perhaps restricted to one particular system. Figure 2-1 presents a simplified block diagram of the DIS. In support of the Simulation Enhancements effort, work has been performed (or is in progress) on models for the platform, sensor (including focal plane and signal processor), scene, and techniques for interfacing the DIS with an in-house image processor for graphics display.

Utilizing the tools developed as a result of the Simulation Enhancements work, the Simulation Applications effort studies issues related to generic surveillance system performance drivers. Typical examples are sensor line-of-sight stability, focal D^* , and critical scene/scenario characteristics such as spectral interval, orbit, scene time-of-day, etc.

2.2 Simulation Enhancements

2.2.1 Platform Simulation

Development of the Integrated Large Space Structures Simulation (ILS³) was begun in 1977 in response to a DARPA need for simulating the optical performance of the HALO system. While intended to be general purpose, the internal structure of the ILS³ (i.e., input, coordinate systems, interpolation methods, contact systems, etc.) was rigidly based on the HALO design. More recently, many analysis efforts have concentrated on single reflector or feedreflector systems. In the absence of a suitable raytrace program to provide the necessary inputs for utilizing the ILS³, alternate special-purpose software packages were developed which did not require a raytrace and which could compute wavefront errors for these simple paraboloidal or spherical systems. While these software packages were adequate for their intended purposes, this approach has three major disadvantages: the packages are problem-specific and must be modified, sometimes extensively, for other applications; no linkage with the DIS is provided; and documentation tends to be scattered and incomplete.

The purpose of the enhancements to the ILS³ is to assemble a package which can be used to analyze both multi-mirror raytraced systems and single surface, paraboloidal or spherical systems. This is being done in five steps: incorporating many of the previously proposed ILS³ changes; incorporating a

general purpose version of the single mirror software; adding a compatible raytrace program; simplifying data communication; and providing linkage to the NASTRAN and DISCOS programs. The use of NASTRAN is important both to provide input to the top level ILS³ modules (dynamics, steady-state, and quasi-static) and in many cases to serve as a replacement for them. These enhancements will provide significant new capabilities for dealing with both infrared and radar systems.

An initial plan has been formulated and preliminary analysis completed to accomplish the above objectives. The remainder of this effort is currently in process.

2.2.2 Sensor Simulation

Many aspects of the focal plane and signal processor models originally in the DIS were specific to the Mini-HALO system. In order to be able to study effectively the capabilities of a generic space-based staring infrared surveillance system, it was necessary to generalize certain aspects of each of these models.

The principal enhancement to the focal plane model was to implement a menu of user-selectable noise models. In addition to the standard noise model corresponding to the basic Mini-HALO focal plane (including saturation and reset features), the user may select that of an ideal focal plane (i.e., scene shot noise only) or may specify either D^* or D^*/D_{BLIP}^* to characterize focal plane noise. In the latter case the user may further specify either a white noise or $1/f$ noise spectrum.

The initial signal processor model in the DIS corresponded to the HALO Signal Processor (HSP). To increase flexibility and modularity, the software architecture for the Signal Processor has been restructured, leaving intact, however, the core HSP algorithm chain. In order to be able to deal with the needs of a general class of space-based staring IR surveillance systems, the character of many of these algorithms has been parameterized, and a number of new algorithms have been added. The focus of much of this activity has been in the following areas: target signature templates; thresholding procedures; threshold level computation and scaling; and "system track" and "acquired track" criteria.

The Sensor Simulation Enhancements are complete at this point and now being used in DIS applications.

2.2.3 Scene Simulation

The single most important initiative undertaken in the Simulation Extensions Project has been the development of an in-house generic scene simulation in order to bring within the scope of the DIS the capability to generate, manipulate and analyze terrestrial scene data sets as functions of the major surveillance system, scenario and mission parameters. This effort has been accomplished by working in conjunction with Photon Research Associates (PRA). Under subcontract to CSDL, PRA is developing a software simulation called GENESIS to meet DIS needs for scene generation and manipulation. The

PRA work is proceeding in two phases: GENESSIS-I, to provide a near-term capability with certain simplifying assumptions and a limited scene data base; and GENESSIS-II, in which all critical scene parameters will be modelled and automated access provided to the DMA/Landsat data base to enable generation of scenes corresponding to any region for which DMA (Defense Mapping Agency) data exists. Tables 2-1 and 2-2 provide a summary of the principal features and current status of GENESSIS-I and GENESSIS-II, respectively. Figure 2-2 presents a simplified block diagram of the GENESSIS software architecture.

2.3 Simulation Applications

The Simulation Enhancements described above have considerably expanded the scope and capability of the DIS to conduct end-to-end performance assessments of space-based staring infrared surveillance systems. As an illustration of this new capability, the DIS has been used to study the effect of choice of spectral interval and selection of scene local time of day on clutter leakage through the signal processor. The basic approach was to begin with the California coast (Santa Cruz) data base and to use GENESSIS to produce two scenes in the 3.6-4.0 μm band and two scenes in the 8.0-9.0 μm band, each pair of scenes corresponding to 8 AM and to noon local time, respectively. A nominal surveillance system mission and configuration were assumed, and the above scenes were processed through the DIS under varying levels of line-of-sight (LOS) jitter. Tables 2-3 and 2-4 summarize the scenario, sensor and signal processor configurations for this investigation. These parameter values reflect the basic configuration for a system whose principal objective is the detection of strategic aircraft against a terrestrial background. The figure of merit used to measure clutter leakage in the signal processor was average number of threshold exceedances per frame. Figure 2-3 illustrates the four scenes used. The spectrum at the bottom of the figure indicates relative temperature (or scene radiance) within each scene.

Since the average number of threshold exceedances per frame is a function of threshold level in the signal processor as well as the level of LOS jitter, the results of this study may be presented from those two points of view. Figure 2-4 shows the dependence on LOS jitter level of the average number of threshold exceedances per frame. The particular threshold level selected is representative of what would be used to acquire a target with a relatively high signal-to-noise ratio. The general trend of the data is such that, for a given level of LOS jitter, higher numbers of exceedances are found in the LWIR band (i.e., 8.0-9.0 μm) than in the SWIR band (i.e., 3.6-4.0 μm). In either band, the higher number of exceedances always occurs at noon local time as opposed to 8 AM.

Figures 2-5 through 2-7 show the dependence of average number of threshold exceedances per frame on threshold level, for progressively increasing values of LOS jitter. Many of the same trends are also evident in this data. Decreasing the threshold results in a rapid increase in threshold exceedances. At a given threshold value, higher numbers of threshold exceedances always occur in the LWIR band as opposed to the SWIR, and, within each band higher numbers of exceedances occur at noon in comparison with 8 AM. Increasing the LOS jitter level results in a translation upward of the curves at higher

Table 2-1. Generic scene simulation Phase I (GENESSIS-I).

FEATURES

- User-specified variables
 - Observer altitude, zenith angle
 - Spectral interval (2.5-13.0 μm)
 - Atmospheric model (LOWTRAN)
 - Field-of-view location (within overall scene)
 - Scene angular resolution
- Five representative terrain data bases
 - California Coast (near Santa Cruz)
 - Brooks Range Mountains of Alaska
 - Arctic Tundra
 - Middle East
 - Central Europe
- Each data base topology extracted from DMA data base
- Each data base registered with Landsat data to obtain materials assignments
 - Limited to 14 material types
- Two representative cloud templates (for superposition over terrain data bases)
- Scene size: 40 km x 40 km

STATUS

- Operational at CSDL

Table 2-2. Generic scene simulation Phase II (GENESSIS-II).

FEATURES

- Enhanced data base
 - Material types expanded to 20
 - Geometrical representations for three additional cloud patterns (Derived from NOAA data)
- GENESSIS/DMA-Landsat interface
 - Software package to automate generation of input data bases from raw DMA and Landsat data
 - Will permit generation of any scenes for which DMA data exists
- Generalized treatment of key atmospheric effects
 - Continuously variable surface-level parameters (e.g., temperature, humidity, wind velocity, skyshine, solar scattering)
- Optimized software architecture
- Detailed user's manual

STATUS

- GENESSIS-II (Part 1) subcontract to PRA currently underway

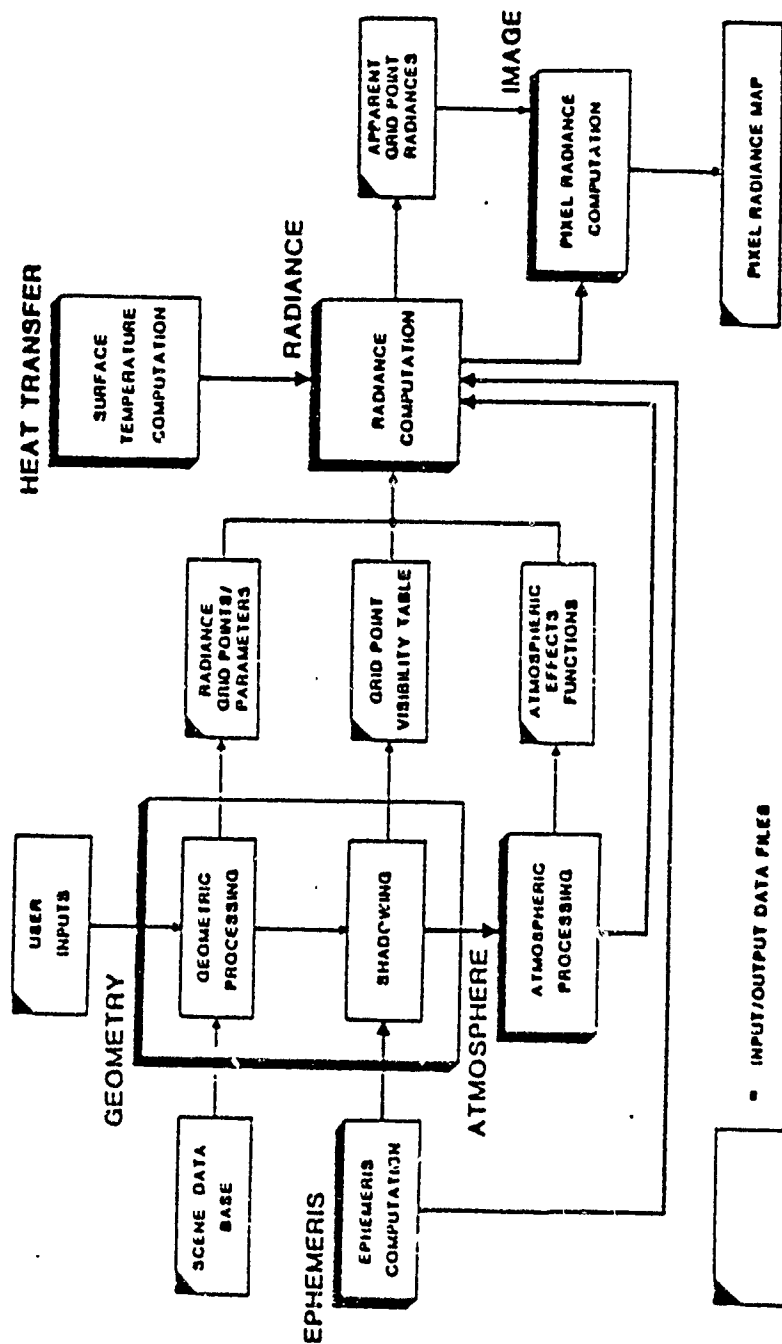


Figure 2-2. GENESIS software architecture simplified block diagram.

Table 2-3. Scenario and sensor specification for GENESSIS Santa Cruz investigation.

PARAMETER	VALUE
<u>Target</u>	None
<u>Backgrounds</u>	
-Location	Santa Cruz (GENESSIS)
-Spectral Bands	3.6-4.0 μm 8.0-9.0 μm
-Times of Day (Local)	8 AM NOON
<u>Spacecraft</u>	
-Drift	None
-Jitter	0.1 $\mu\text{rad rms}$ 0.5 $\mu\text{rad rms}$ 1.0 $\mu\text{rad rms}$
-Altitude	35,700 km
-Boresight	NADIR
<u>Optics</u>	
-Aperture Diameter	1.4 m
-Obscuration Ratio	0.35
-Thruput	0.135
-Point-spread Function	Gaussian ($\sigma = 5.01 \mu\text{rad}$)
<u>Focal Plane</u>	
-Detector Geometry	25 x 25 Array of 100 μm (20 μrad) Square Pixels
-Frame Duration	3.4 sec
-D*	$2.8 (10)^{12} \text{ cm } \sqrt{\text{Hz/W}}$
-Responsivity non-uniformity	
.Fixed Pattern	0%
.Random	15%

Table 2-4. Signal processor configuration for GENESSIS
Santa Cruz investigation.

PARAMETER	VALUE
Difference Filter	3rd Order
Threshold Level	User Input
Assumed Target Contrast	Negative
Threshold Templates	CSDL MTD
Threshold Algorithm	CSDL Rationalized Exceedance Thresh- olding (Version 1)
Cluster Basis	Threshold Exceedances
Centroid Basis	Threshold Exceedances
System Track Criterion	3 out of 3
Acquired Track Criterion	10 out of 12
System Track Threshold Scaling	0.5
Least Squares Track Linearity Criterion	± 1.8 Pixels



Figure 2-3. Composite of GENESIS Santa Cruz scenes.

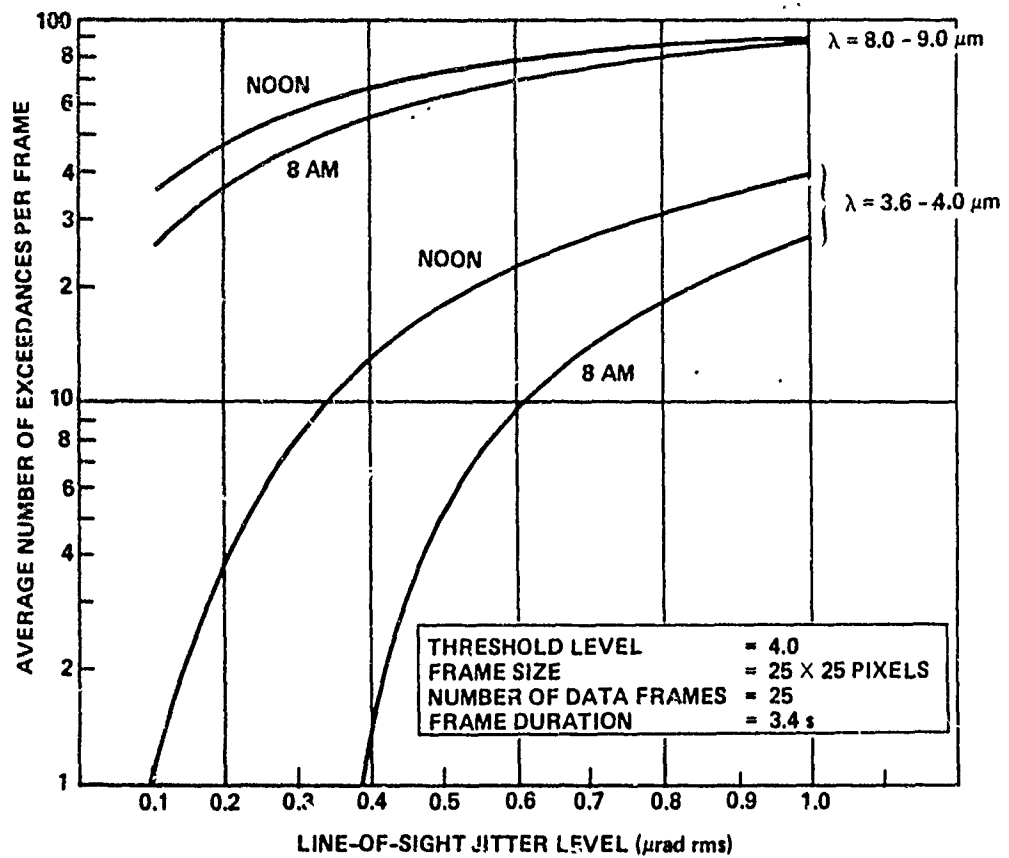


Figure 2-4. Average clutter leakage as a function of line-of-sight jitter level for the GENESSIS Santa Cruz scene, with local time-of-day and spectral band as parameters.

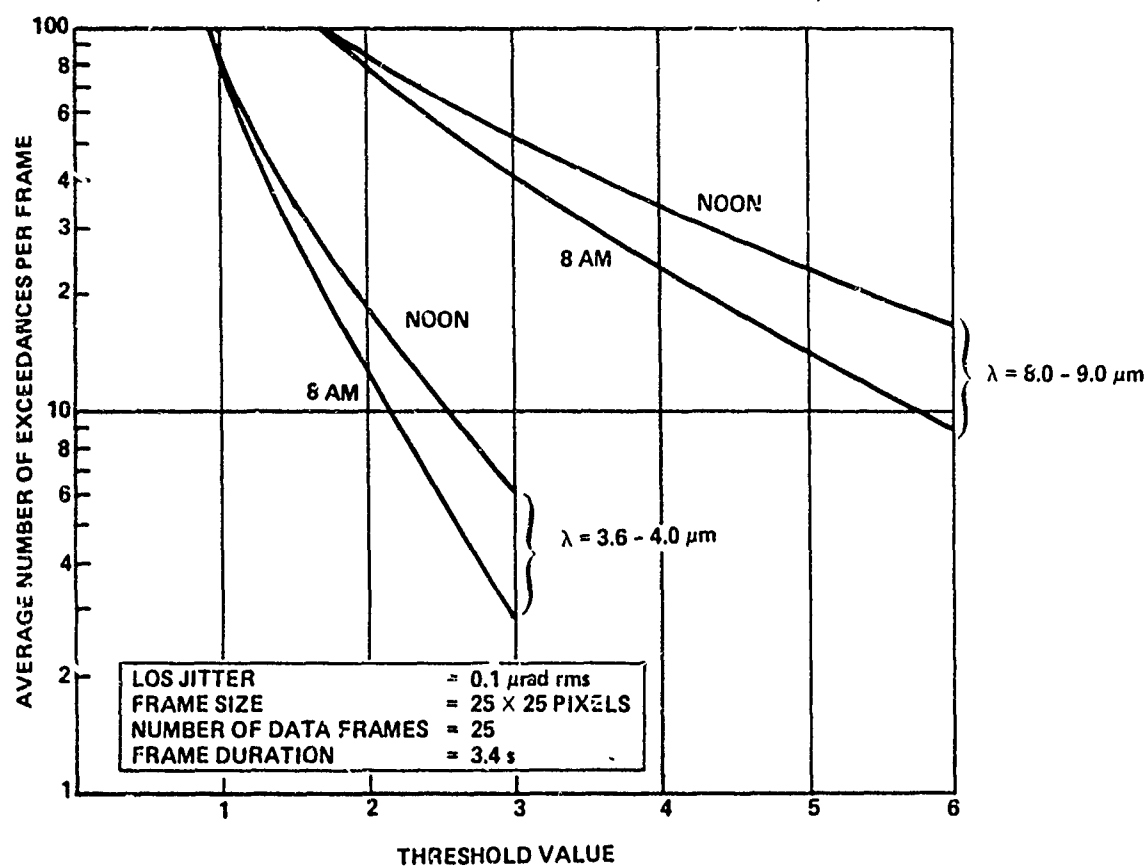


Figure 2-5. Average clutter leakage as a function of threshold level for the GENESSIS Santa Cruz scene, with local time of day and spectral band as parameters. (LOS Jitter = $0.1 \mu\text{rad RMS}$)

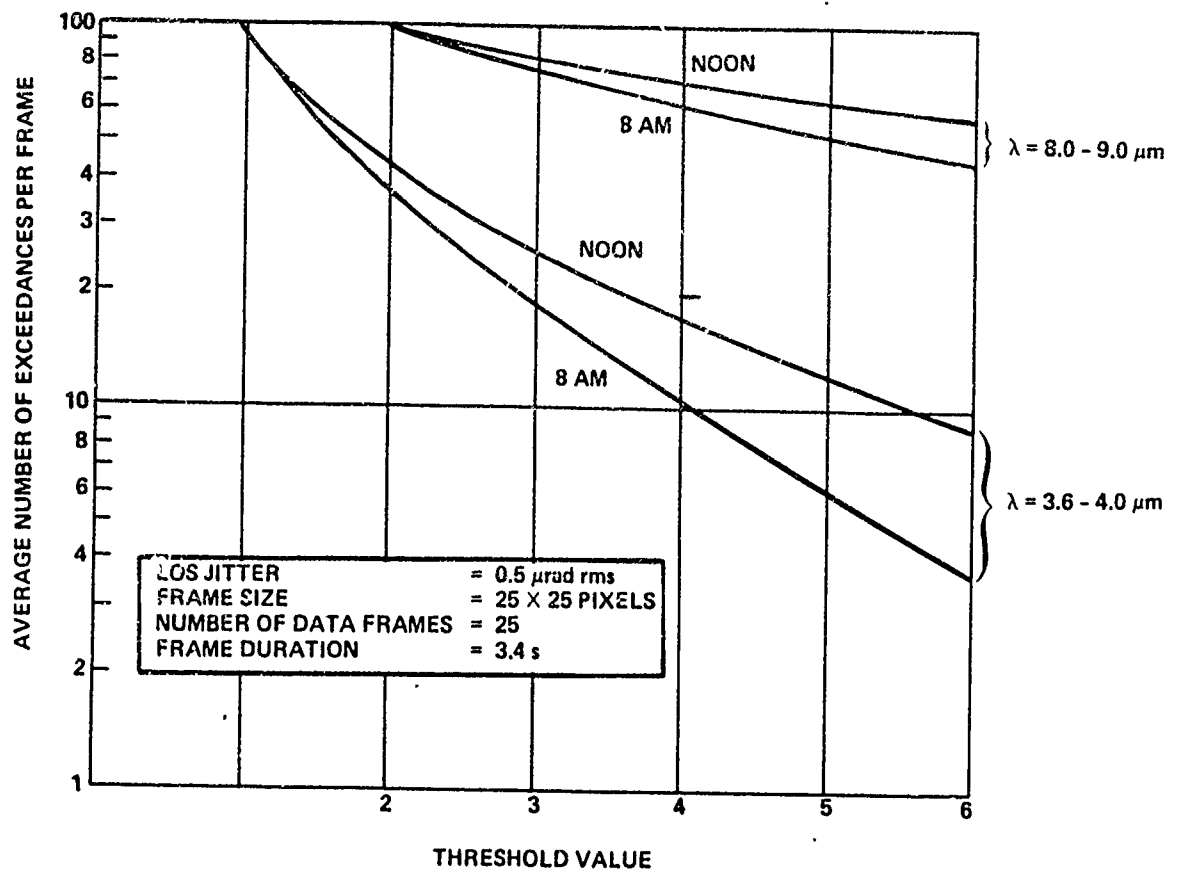


Figure 2-6. Average clutter leakage as a function of threshold level for the GENESIS Santa Cruz scene with local time of day and spectral band as parameters. (LOS Jitter = $0.5 \mu\text{rad RMS}$)

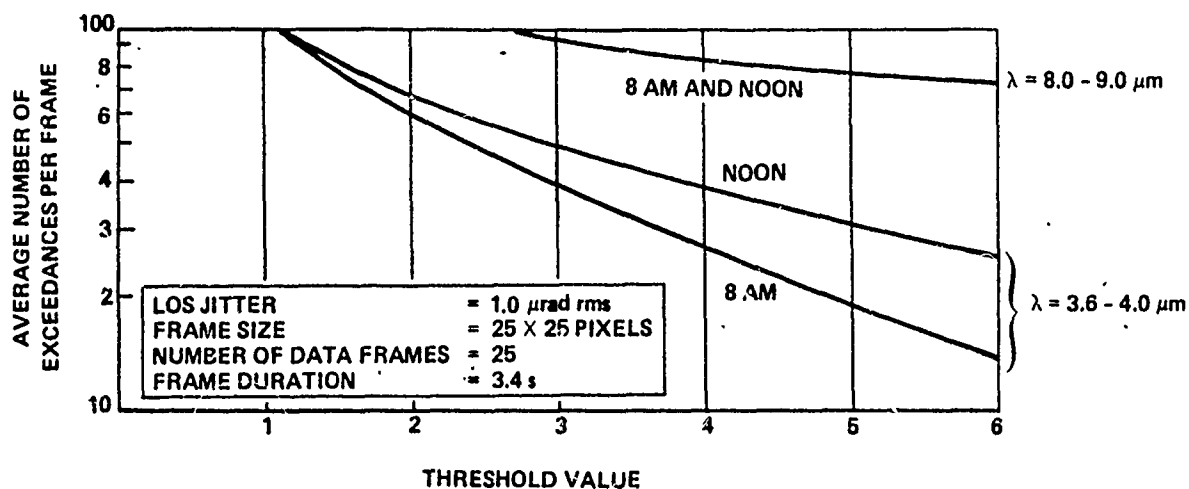


Figure 2-7. Average clutter leakage as a function of threshold level for the GENESSIS Santa Cruz scene, with local time of day and spectral band as parameters. (LOS Jitter = $1.0 \mu\text{rad RMS}$)

threshold values, as can be seen by comparing Figures 2-5 and 2-6. In addition, there is a compression within each spectral band of the exceedance curves corresponding to noon and to 8 AM. In Figure 2-7, an LOS jitter level of 1.0 μ rad RMS (ten times the value used in Figure 2-5) results in the coalescing of these two curves for the LWIR band.

A subject of great interest in the study of signal processor performance and scene/sensor interaction is a determination of the conditions under which false target tracks arise. Figure 2-8 summarizes graphically the false tracks which resulted during the course of the present study. Separate numbers, i.e., "1" versus "2", are used to designate the relative position of distinct tracks within the overall 25 x 25 pixel field-of-view. Consistent with the data presented in Figures 2-4 through 2-7, false tracks were found at low threshold levels where the average number of exceedances is very high. Under these conditions the likelihood of a time sequence of individual exceedances occurring in such a fashion as to satisfy the signal processor track formation and acquisition criteria is considerably increased.

2.4 Conclusions

The focal plane and signal processor simulation enhancements are complete, and the platform simulation enhancements are in process and proceeding satisfactorily. Phase I of the Generic Scene Simulation (GENESIS) activity is complete and operational at CSDL. The last phase of this activity is currently in process under subcontract to CSDL at Photon Research Associates. The Draper Integrated Simulations thus represent a highly sophisticated tool for end-to-end performance trade-offs of a variety of space-based systems, and especially staring mosaic IR surveillance systems.

LOS-induced clutter leakage through the signal processor has been simulated as a function of spectral interval and scene time-of-day for a generic staring mosaic IR surveillance system. The functional dependence of the scene/sensor interaction is complex and has been described quantitatively by a series of curves showing average number of threshold exceedances per frame both as a function of LOS jitter for a particular threshold and as a function of threshold for particular LOS jitter values. Qualitatively it is clear that increased LOS jitter yields increased clutter leakage in all cases considered. Clutter leakage in the short-wave infrared (SWIR) band of 3.6-4.0 μ m is significantly less than in the long-wave infrared (LWIR) band of 8.0-9.0 μ m. For either SWIR or LWIR, clutter leakage at noon (local time) is greater than early morning. For a fixed threshold value, increased LOS jitter drives early morning clutter levels toward noon clutter levels in both the SWIR and the LWIR bands. And, finally, low threshold values in the presence of LOS jitter can result in the generation of false acquired tracks.

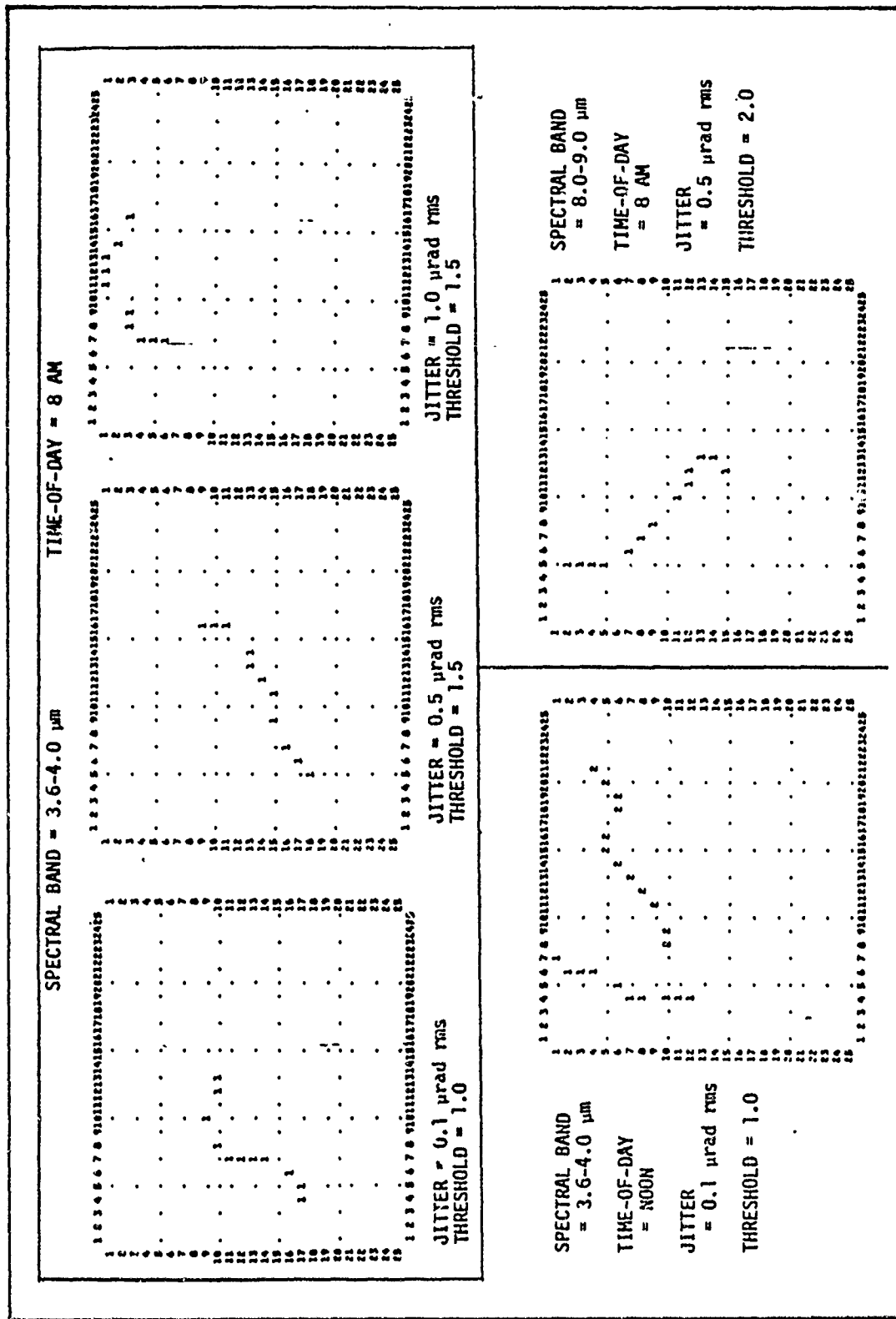


Figure 2-8. False tracks induced by LOS jitter in the GENESIS Santa Cruz scene.

SECTION 3

HALO OPTICS DECONVOLUTION TEST

3.1 Introduction

HALO is a multi-mirror large optical imaging system with a wide field of view. To maintain alignment as well as image quality, the mirrors are actively controlled with actuators. The term "deconvolution" implies a sensing and control scheme by which a deformed HALO optical system is corrected in near real time. In one of the techniques worked on by the Itek Corporation, the wavefront errors of the deformed system are measured with a wavefront sensor for several object points near the edge of the field-of-view of the system. The wavefront sensor is placed around the focal plane. The wavefront errors are decomposed into mirror figure errors and actuator displacements are generated to correct them with a deconvolution algorithm. This report describes a limited blind test that CSDL prepared for Itek to test and validate this algorithm. We conclude that the algorithm successfully determined the actuator displacements from the wavefront errors.

3.2 Optical System for Deconvolution Test

For a hardware demonstration of their deconvolution algorithm, Itek has been planning to use an optical imaging system consisting of three active flat mirrors and a pair of lens doublets mounted back-to-back in a 1:1 magnification. A schematic of this system is shown in Figure 3-1.

The lenses are the imaging elements of the system, and the mirrors are the deformable elements. Aberrations are introduced into the system by deforming the mirrors. The active mirrors, thus simulate the deformable aspects of a HALO system. The footprints on the mirrors of rays from a given point object are similar to those on the S-HALO or WALRUS mirrors. A perspective view of the optical system is given in Figure 3-2. It shows the coordinate system chosen to designate the actuator and ray distributions.

3.3 Actuator Distribution and Influence Function

Each of the three mirrors has 37 actuators distributed on an equilateral triangular lattice as shown in Figure 3-3. In consultation with Itek, the influence function of the actuators was chosen to be similar to the one for active mirrors developed for the compensated imaging program. This influence function is given by

$$\begin{aligned} f(r) &= \left[1 - 1.2(r/d)^2 \right]^2, & r &\leq d/\sqrt{1.2}, \\ &= 0, & r &> d/\sqrt{1.2}, \end{aligned}$$

where

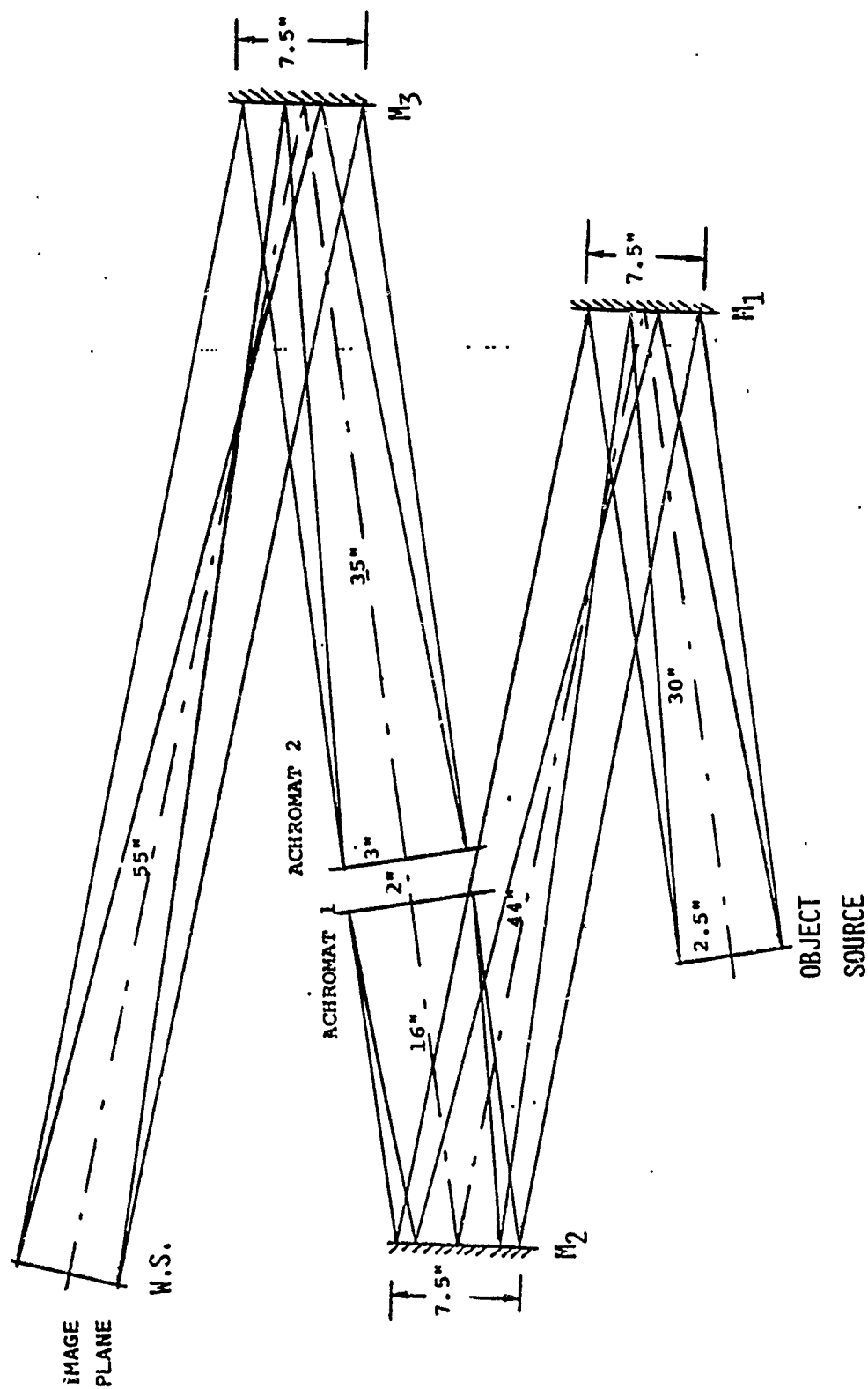


Figure 3-1. Schematic of the optical system used for the deconvolution test. The lenses are the imaging elements and the three active mirrors simulate the deformable aspects of a IHALO system.

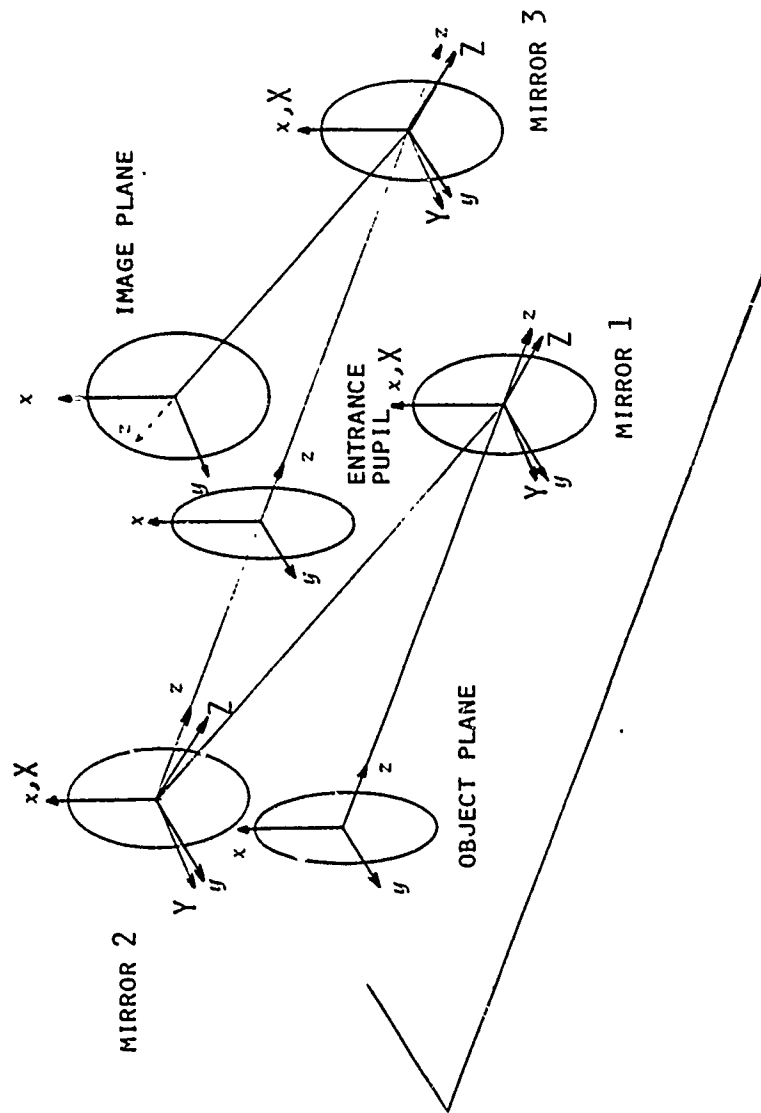


Figure 3-2. Perspective view of the optical system illustrating the coordinate system used for actuator and ray distributions. (X, Y, Z) is the coordinate system used to describe mirror deformations. (x, y, z) is the coordinate system used for ray tracing.

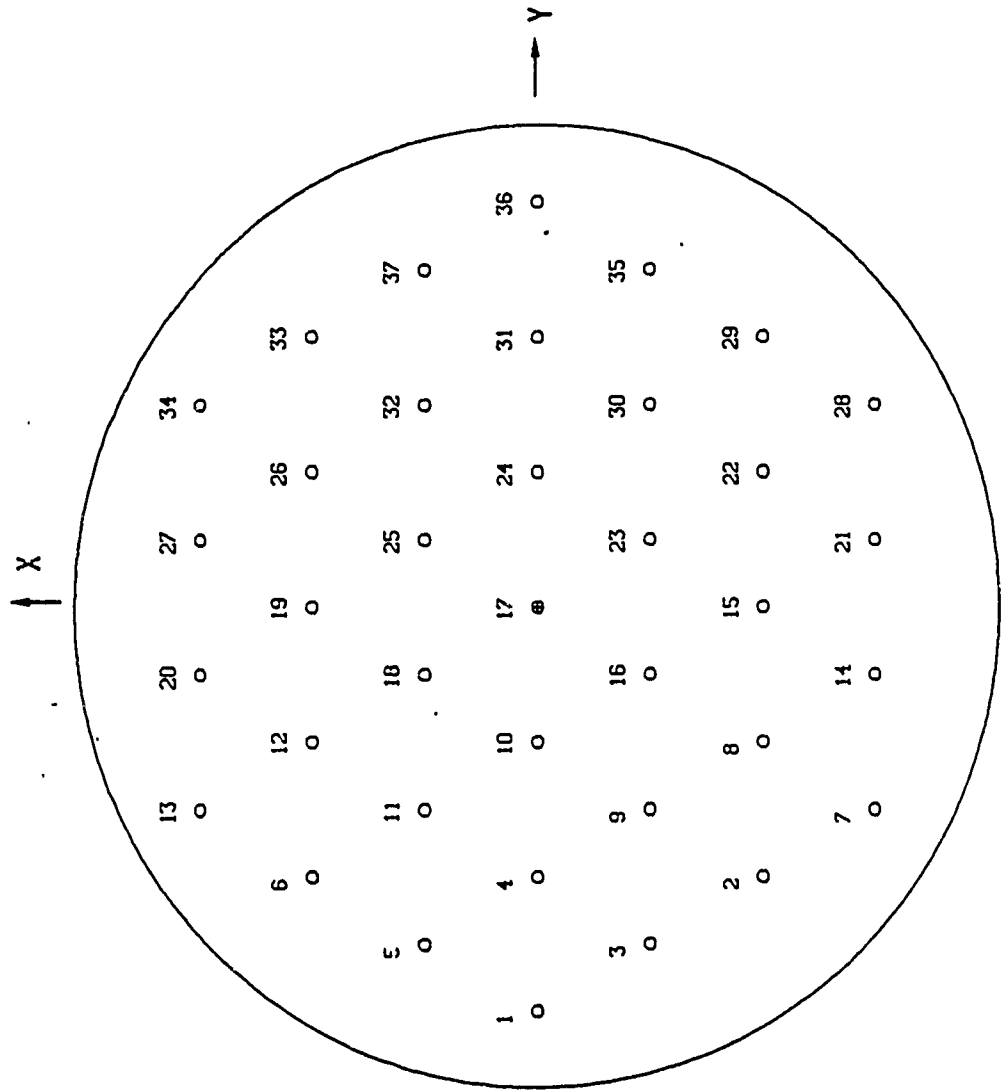


Figure 3-3. Actuator distribution on mirrors.

r = distance from the actuator,
 d = actuator spacing.

The variation of $f(r)$ with r is shown in Figure 3-4. It is noted that the influence function is radially symmetrical about the actuator position. Moreover, one actuator does not produce any influence on another. The factor of 1.2 was chosen to minimize the effect of quilting when all actuators are displaced by the same amount. With a 1.2 factor, quilting is at most 8%. When an actuator is displaced by an amount h , the deformation produced in the mirror is given by $hf(r)$. In our problem $d \approx 3\text{cm}$.

3.4 Mirror Deformations

The deformations of the mirrors used in the deconvolution test are given in Figure 3-5. The numbers in this figure give the actuator displacements in units of $\lambda/100$. Mirror M_1 was deformed according to cryogenic deformations of an Itek HALO mirror. Mirror M_2 has deformations described by Zernike polynomials representing coma and astigmatism. Mirror M_3 was given a rigid-body displacement along its normal. The mean, peak-to-peak, and standard deviation of the actuator displacements are indicated in the figure for each mirror.

3.5 Selection of Point Objects

Nine point objects were selected for ray tracing and determining the system wavefront errors. Eight of these are uniformly distributed around the edge of the field-of-view of the system (1.5° from the axis), and one is placed on the system axis as indicated in Figure 3-6. The on-axis point object was used only for the sake of completeness to include the deformations of the central portion of mirror M_1 . The wavefront sensors placed around the focal plane cannot sense the effect of these deformations. In practice, the central portion of M_1 will, for example, be corrected by CSDL's image sharpening approach.^{1,2}

3.6 Mirror Footprints

Figure 3-7 shows the footprint on the mirrors of the image forming rays from point objects 1 and 2. We note that, as in a HALO optical system, the footprints of rays from point objects such as 2, near the edge of the field of view, on mirrors M_1 and M_2 cover the mirror portions used in imaging. However, their footprint on mirror M_1 is not only small compared to the mirror size, but also it is off the mirror center. Accordingly, the footprints of the rays from the 8 off-axis point objects cover the outer portion of the mirror M_1 but not its central portion.

The image of the on-axis point object is formed at the center of the focal plane. The central portion of mirror M_1 can be corrected by the image sharpening technique using the focal plane data.

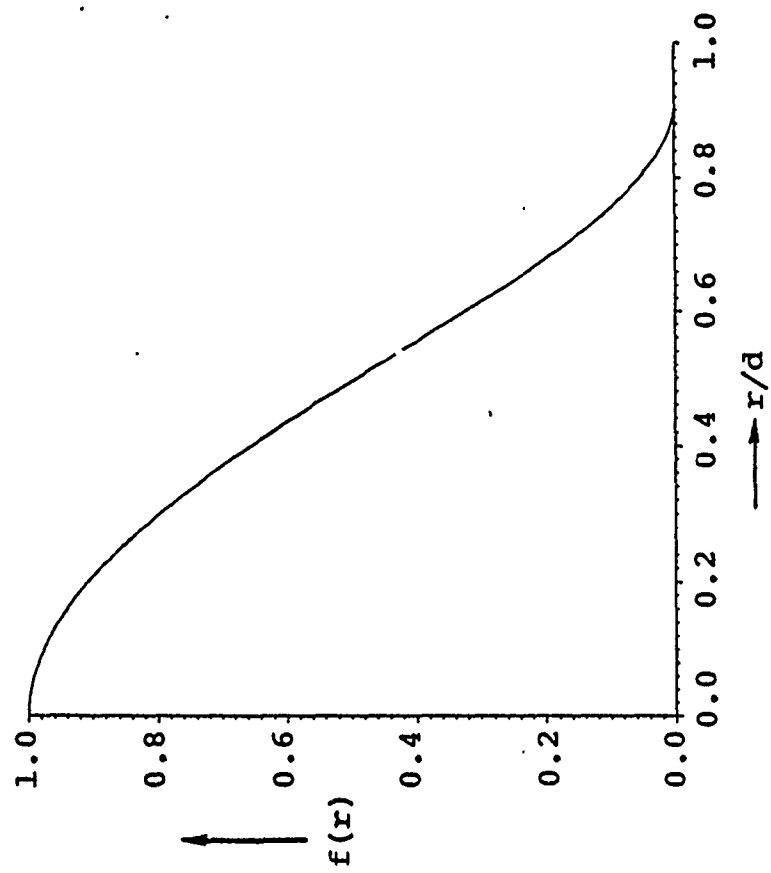


Figure 3-4. Actuator influence function.

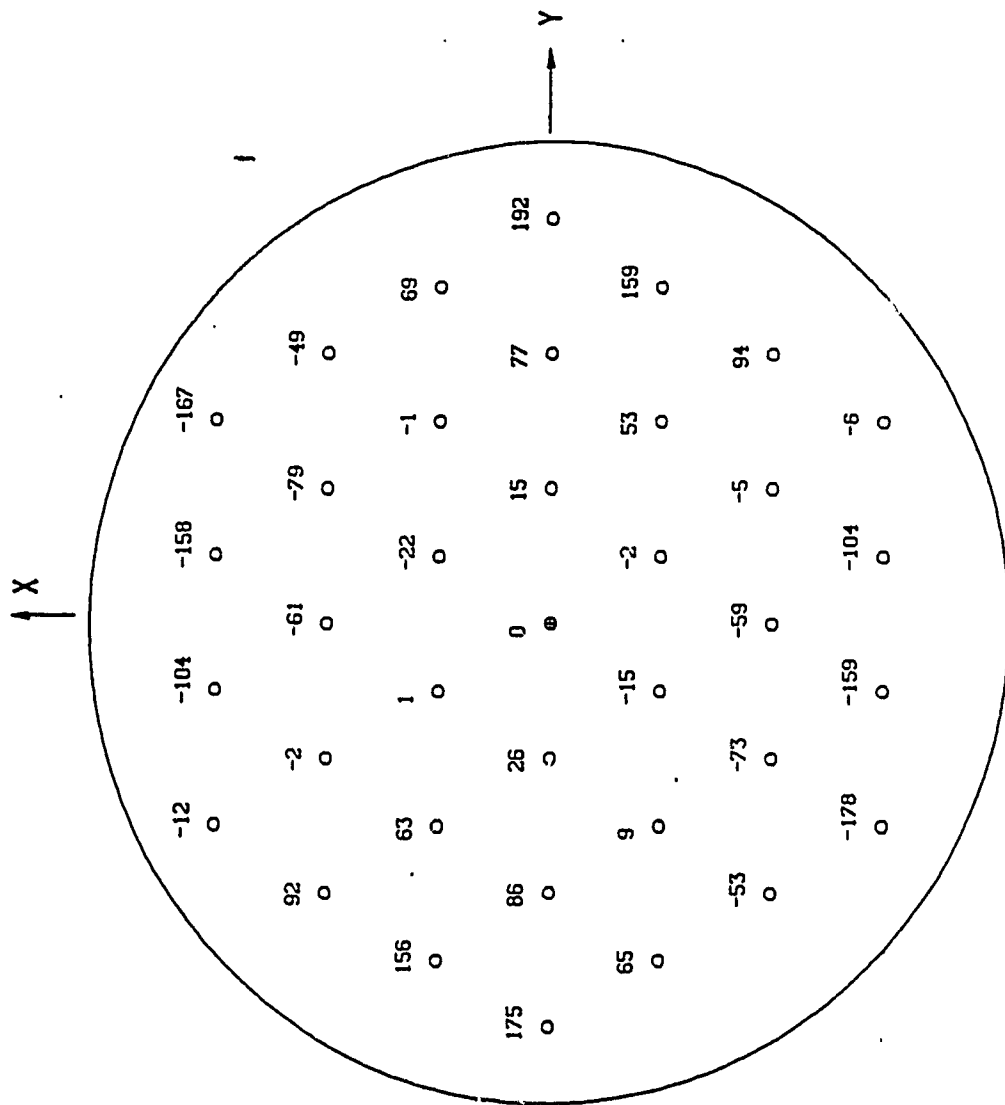


Figure 3-5b. Mirror 2. $\sigma_D = 94$, $D_{\text{mean}} = 0$, $D_{p-p} = 371$.

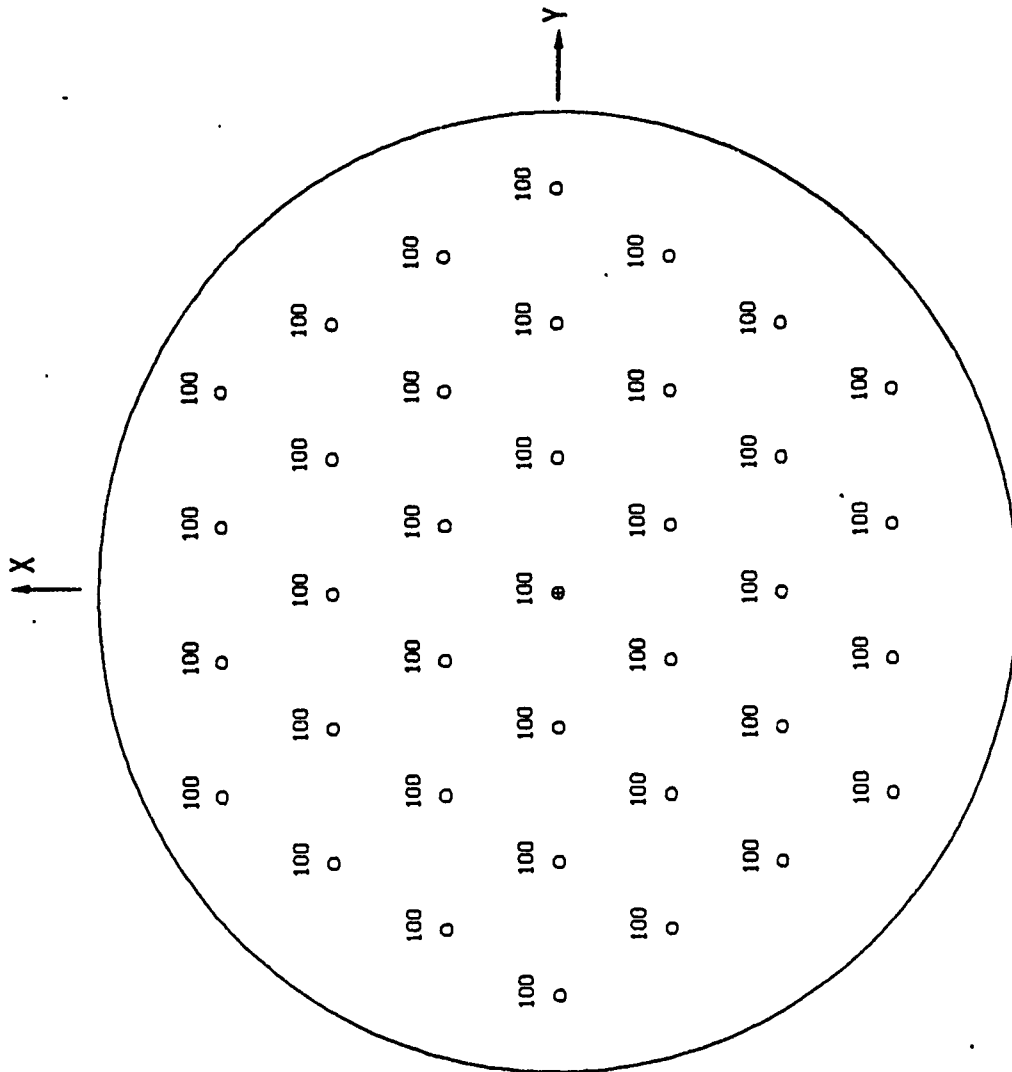


Figure 3-5c. Mirror 3. $\sigma_D = 100$, $D_{\text{mean}} = 100$, $D_{p-p} = 100$.

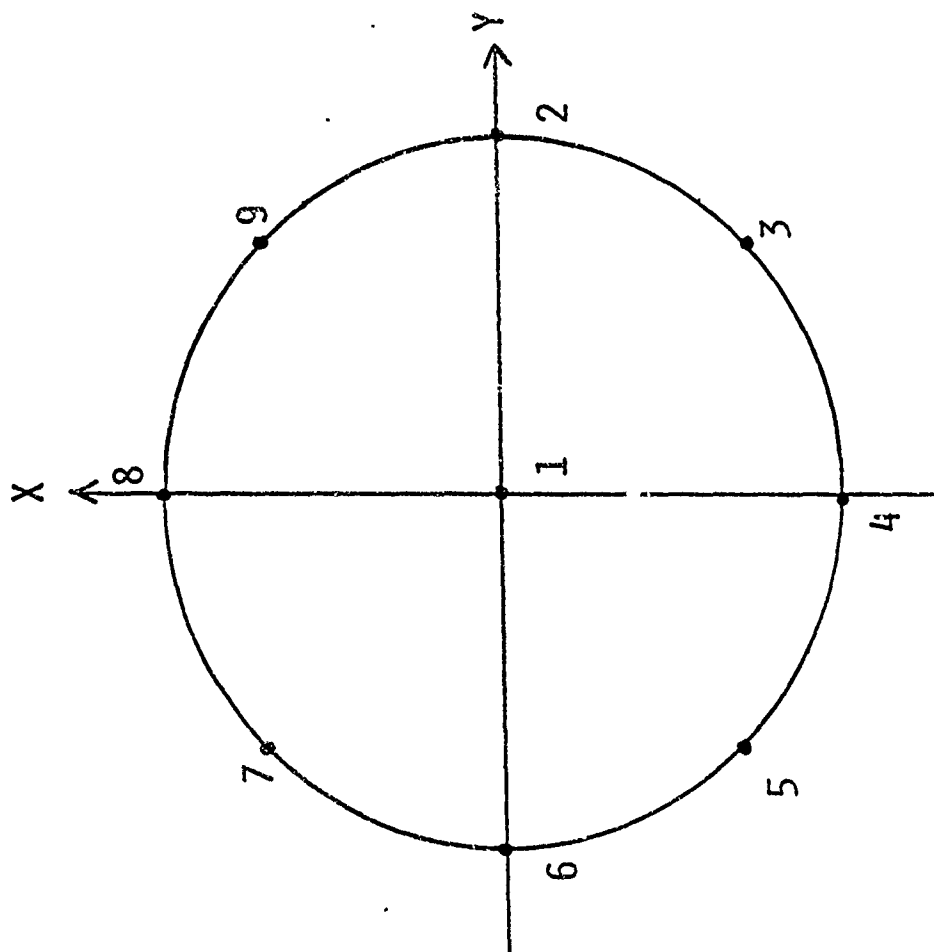


Figure 3-6. Distribution of point objects used for determining system wavefront errors.

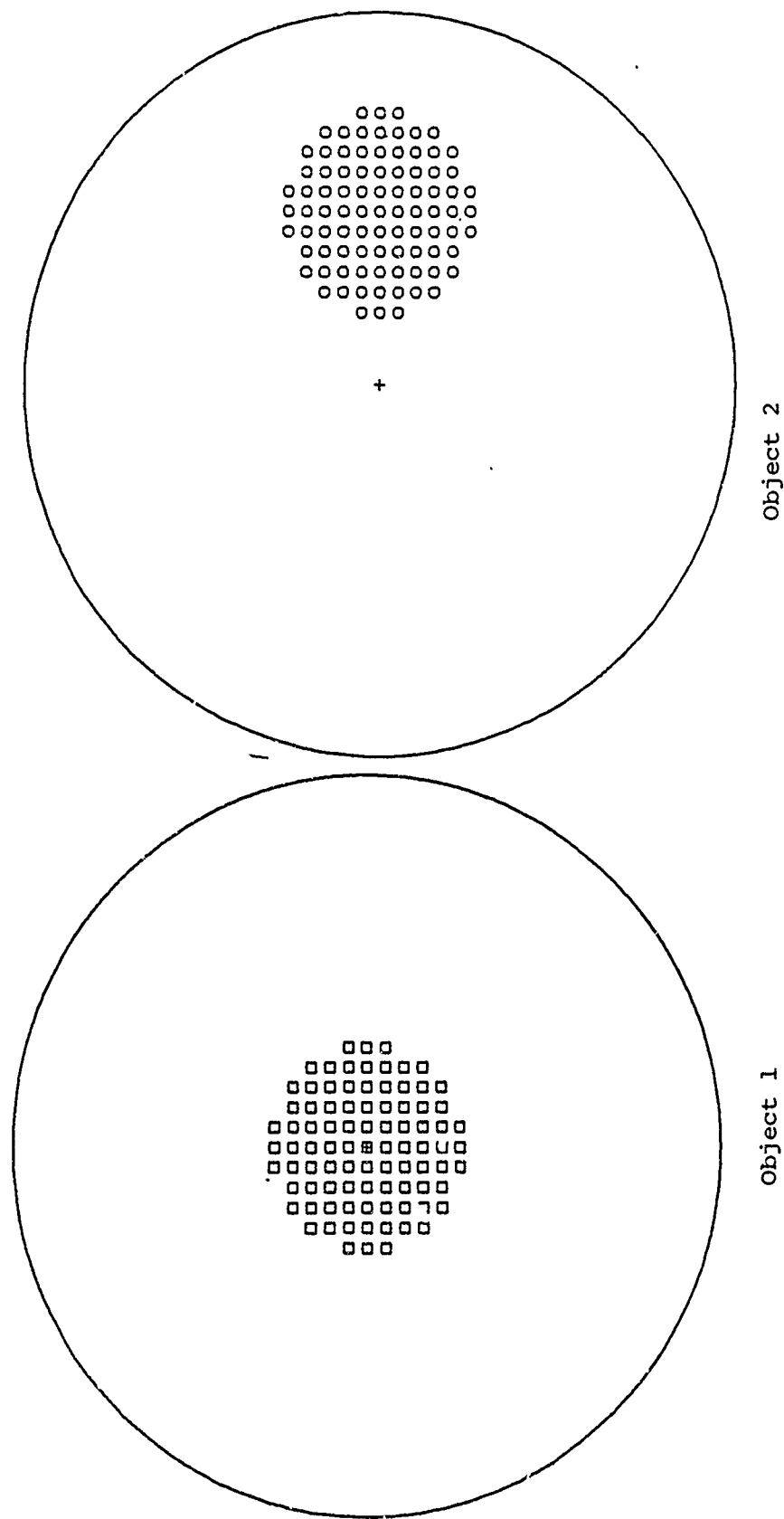
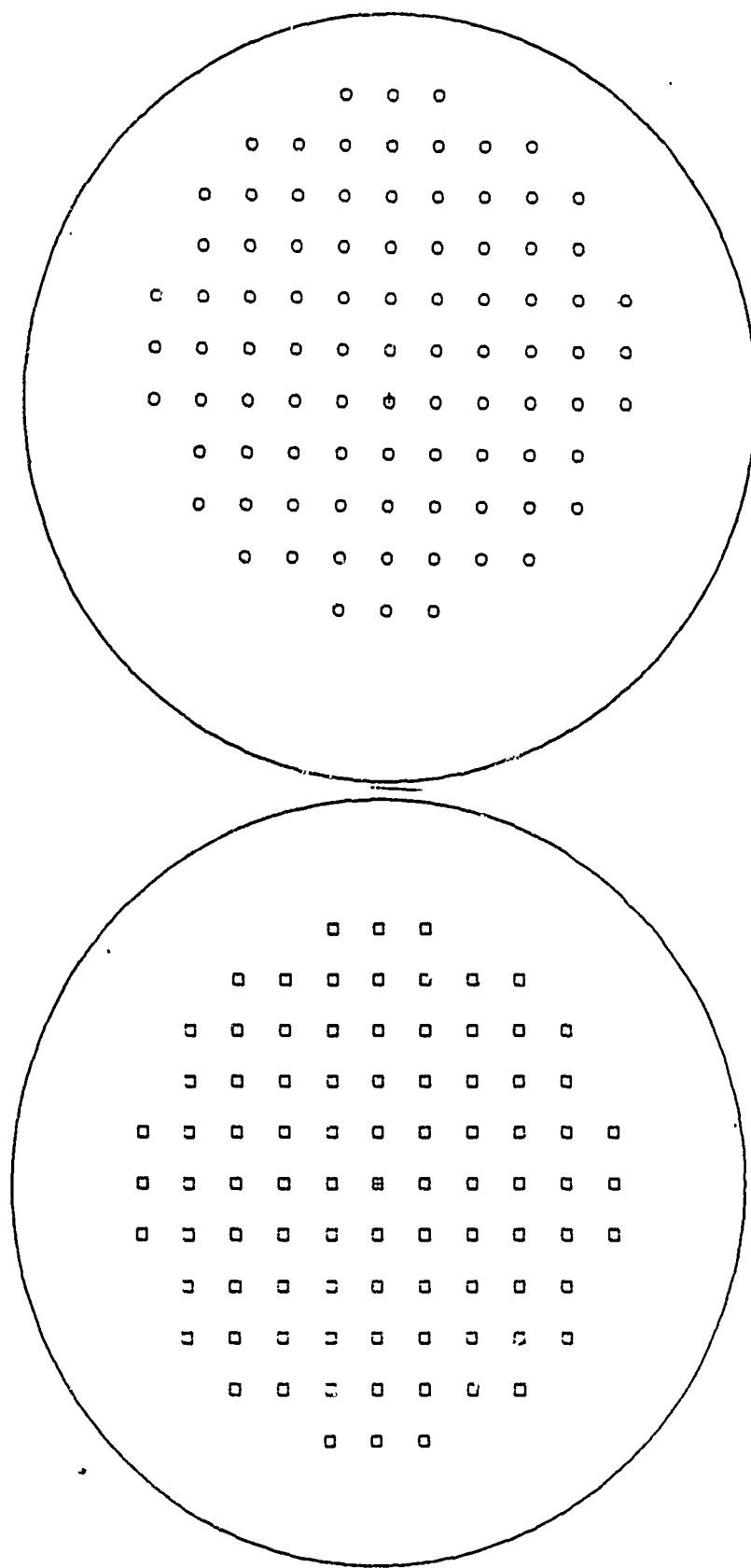


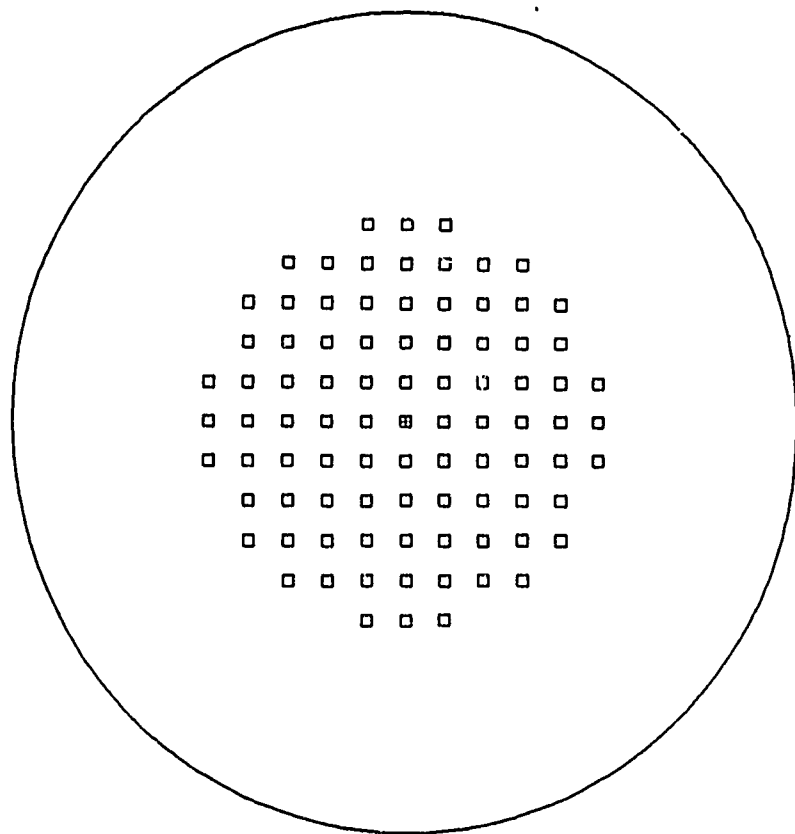
Figure 3-7. Footprints of image forming rays on mirrors.
a. Mirror 1.



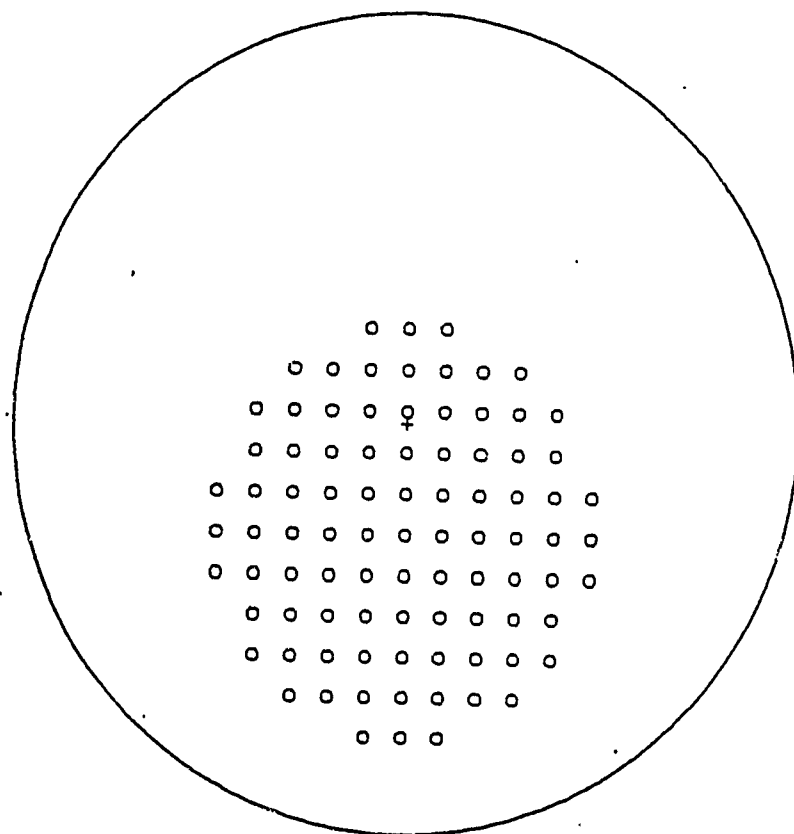
Object 1

Object 2

Figure 3-7b. Mirror 2.



Object 1



Object 2

Figure 3-7c. Mirror 3.

3.7 Wavefront Errors

When the optical system deforms, the wavefront error introduced at a certain point on the wavefront is given by the change in the path length of a ray passing through that point. The change in the path length of a ray from a given point object in terms of the mirror deformations is given according to³

$$\Delta W_i = 2 \sum_{m=1}^3 \hat{n}_{im} \cdot \delta \vec{r}_{im} \cos \theta_{im},$$

where

\hat{n}_{im} = unit vector along the normal to the surface of undeformed mirror m at the point of incidence of the ray i,

$\delta \vec{r}_{im}$ = displacement of the point of incidence of ray i on mirror m,

θ_{im} = angle of incidence of ray i on the undeformed mirror m.

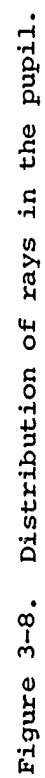
Since we are dealing with flat mirrors, n_{im} for a given mirror is independent of i.

Figure 3-8 shows the distribution of 89 rays in the pupil used for determining the wavefront errors. The wavefront errors corresponding to point objects 1 and 2 when the optical system is deformed according to mirror deformations of Figure 3-5 are given in Figure 3-9. These wavefront errors include $\lambda/20$ random error to simulate the noise of a wavefront sensor. We provided Itek with noisy wavefront errors at 89 points for each of the nine point objects.

3.8 Test Results

3.8.1 Mirror Deformations

From the wavefront error data for the nine point objects we provided to Itek, they determined the actuator corrections (displacements) required to correct the figure of the mirrors to reduce the wavefront errors. The actuator corrections determined by their deconvolution algorithm are given in Figure 3-10. The residual errors obtained by subtracting these corrections from the errors given in Figure 3-5 are also shown in Figure 3-10. The mean and the standard deviation of the residual displacements are listed in the figure for each of the three mirrors. We note that the residual errors are quite small except for the corner actuators. The region of mirrors where corner actuators are located is not used for imaging. Hence, the effect of these actuators on the mirror figure is not observed by the wavefront sensor.



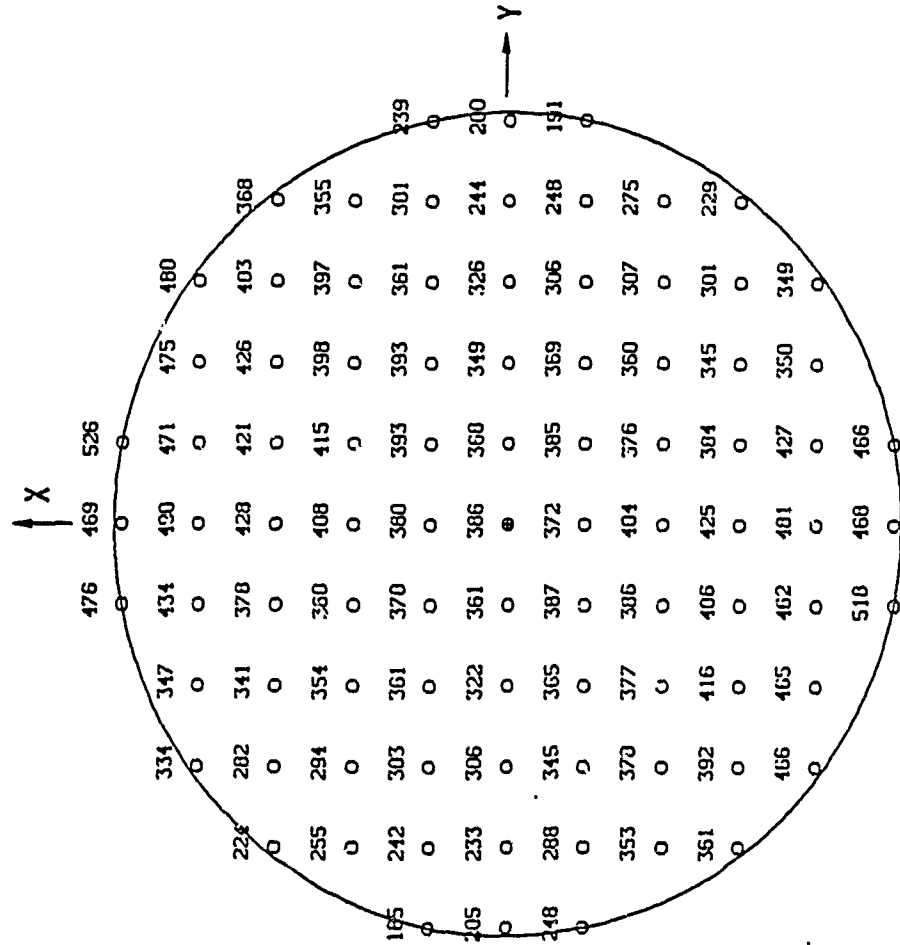
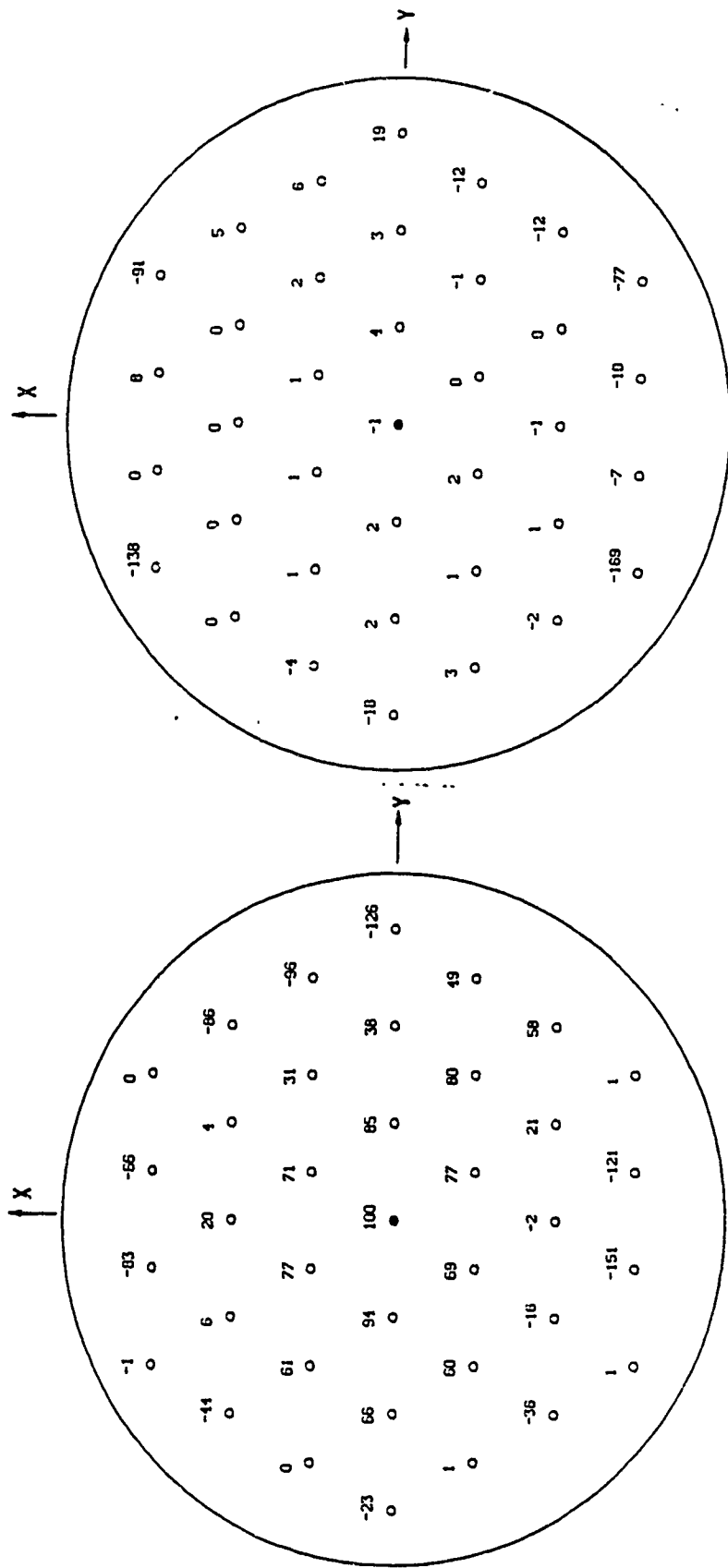


Figure 3-9. Wavefront errors with noise in units of /100
a. Object 1. $\sigma_w = 78$, $w_{\text{mean}} = 362$, $w_{p-p} = 200$.



Figure 3-9b. Object 2. $\sigma_W = 106$, $w_{\text{mean}} = 303$, $w_{p-p} = 237$.



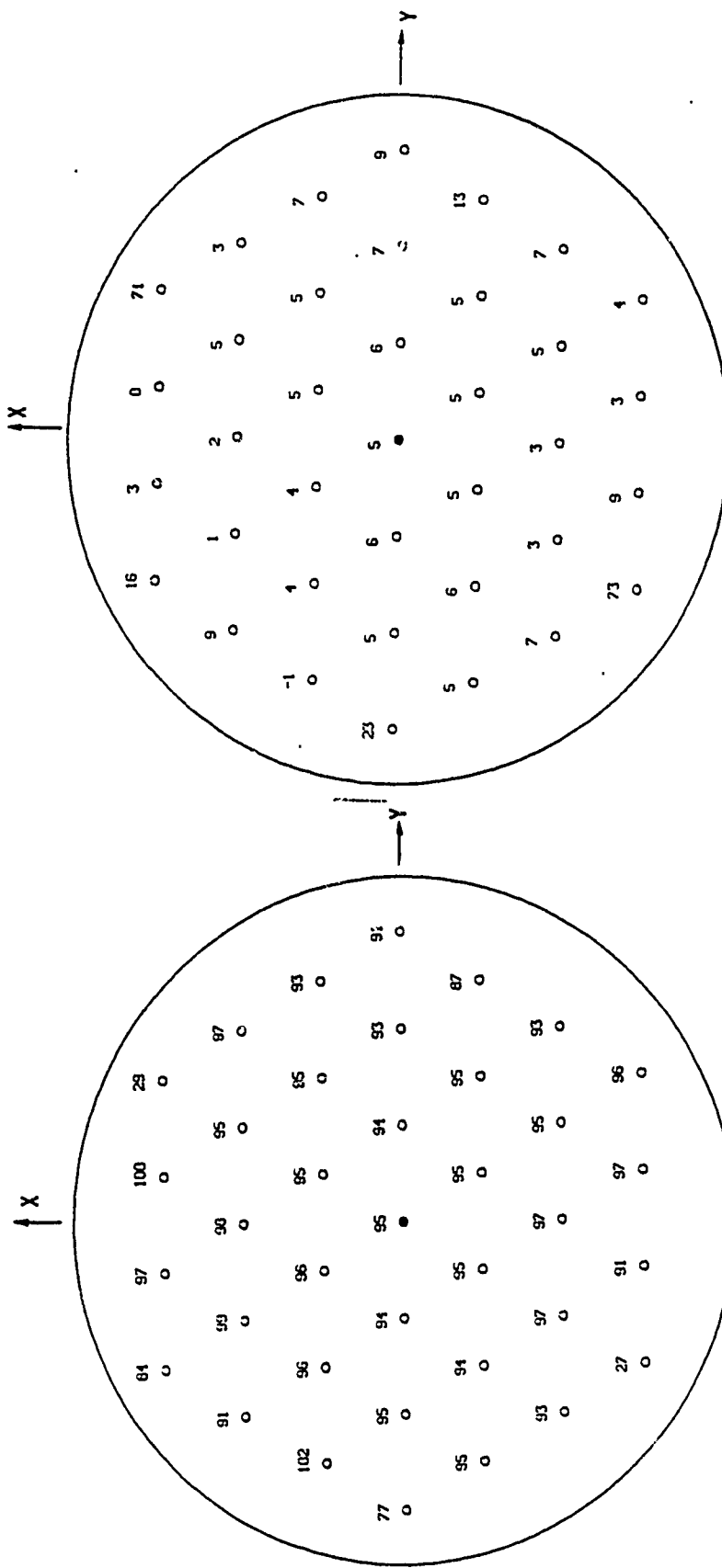
Corrections

$\sigma_D = 66$, $D_{\text{mean}} = 66$

Residual Errors

$\sigma_D = 39$, $D_{\text{mean}} = -13$

Figure 3-10. Actuator corrections and residual errors (in units of $\lambda/100$).
a. Mirror 1.



Corrections

$$\sigma_D = 16, D_{\text{mean}} = 91$$

Residual Errors

$$\sigma_D = 16, D_{\text{mean}} = 9$$

Figure 3-10c. Mirror 3.

3.8.2 Wavefront Errors

The wavefront errors of the corrected system were determined by tracing 89 rays as in the case of the deformed system. These errors were quite small ($\sigma_w < \lambda/40$) indicating an excellent correction. Random noise of $\lambda/20$ was added to these errors to simulate the wavefront errors that a wavefront sensor would measure. The noisy residual wavefront errors for point objects 1 and 2 are shown in Figure 3-11. The mean, peak-to-peak, and standard deviation of the wavefront errors are also given. It is evident from the standard deviation that most of the error is indeed due to the wavefront sensor.

3.8.3 Point-Spread Functions

The aberrated and the corrected point-spread functions for point objects 1 and 2 are shown in Figures 3-12 and 3-13, respectively. The standard deviation of the aberration, the Strehl ratio (aberrated irradiance at the center relative to its unaberrated value) and peak irradiance are also given in the figures. For example, for point object 1, the deformed system gives a Strehl ratio of only 0.025. The light is spread over a region $31\lambda F$ wide compared with approximately $2\lambda F$ for the corrected (or aberration-free) system. With a correction determined by Itek deconvolution algorithm, a Strehl ratio of approximately 0.95 is obtained. The corrected Strehl ratios in Figures 3-12 and 3-13 are slightly lower because of the wavefront sensor noise.

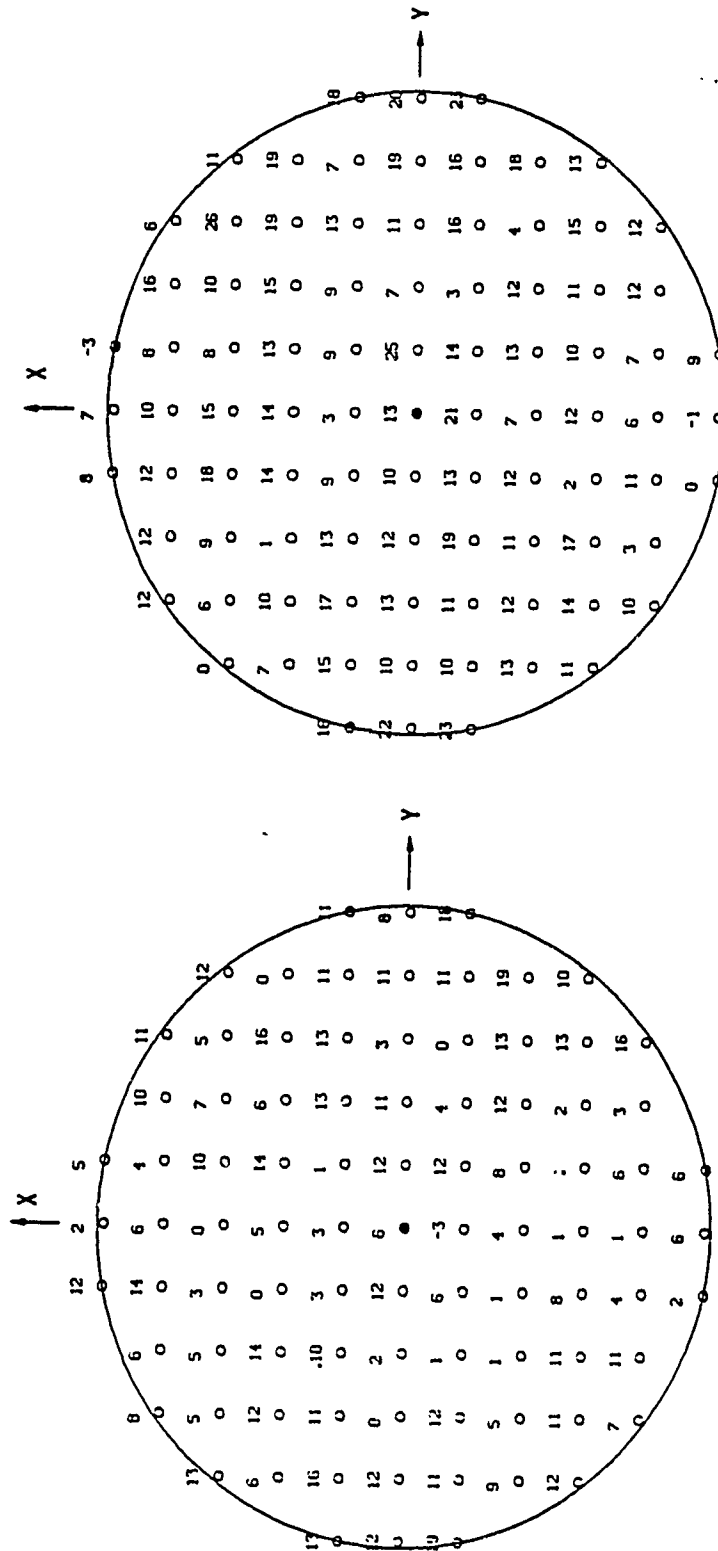
3.9 Discussion, Conclusions, and Recommendations

An optical system using three flat mirrors as deformable elements has been used for testing the deconvolution algorithm developed by Itek. Each mirror has 37 actuators, and 89 rays have been used to determine wavefront errors of a deformed system. CSDL provided Itek with a known-deformation test and a blind test. The known-deformation test was prepared so that CSDL and Itek softwares could be tested for compatibility. On the blind test, two of the 9 wavefronts that Itek was given are shown in Figure 3-9.

Itek's deconvolution algorithm determined the actuator displacements on each mirror and these were subtracted from the input displacements given in Figure 3-5. The corrected system was ray-traced to determine its imaging quality. It gave a Strehl ratio of approximately 0.9 indicating an excellent correction.

We conclude that Itek's deconvolution algorithm successfully determined the actuator displacements from the wavefront errors. The residual wavefront errors were negligibly small and below the wavefront sensor noise.

We recommend that one more blind test be prepared for Itek's deconvolution algorithm to include more realism. Some of the desirable features of this test are listed below.

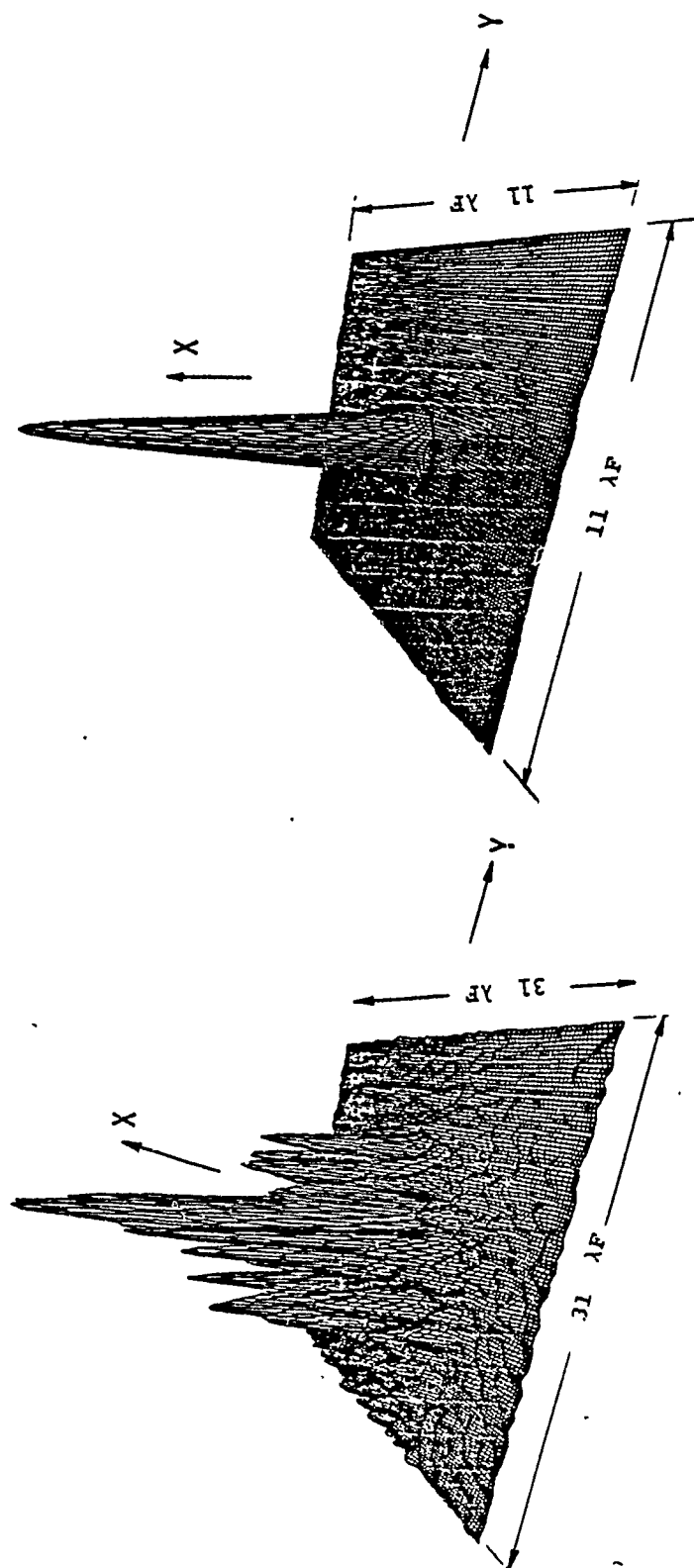


Object 2

Object 1

$\sigma_W = 5, W_{\text{mean}} = 8, W_{p-p} = 22$ $\sigma_W = 6, W_{\text{mean}} = 12, W_{p-p} = 28$

Figure 3-11. Residual wavefront errors (in units of $\lambda/100$).



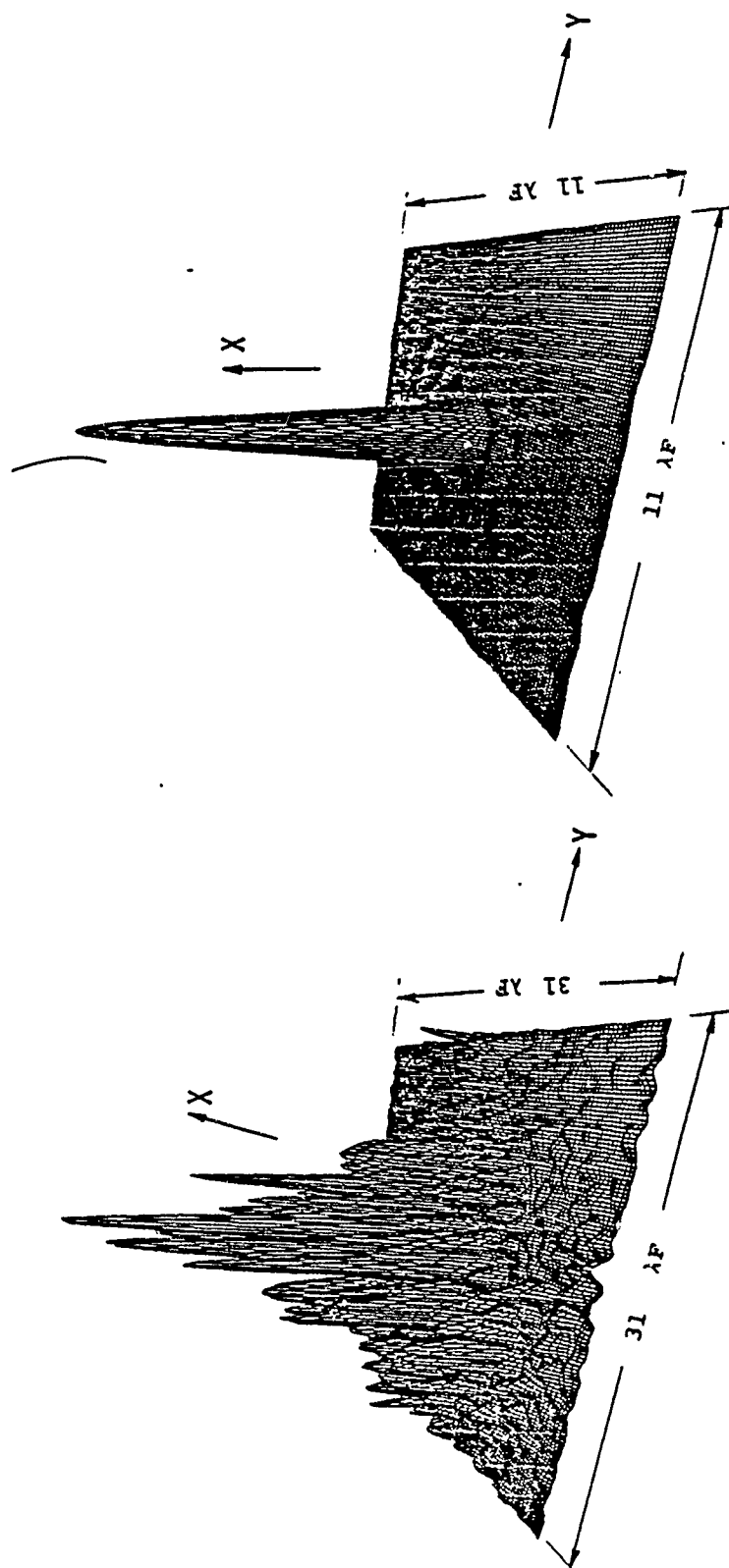
Aberrated

Corrected

$\sigma_w = 0.78\lambda$, Strehl = 0.025, Peak = 0.047

$\sigma_w = 0.051\lambda$, Strehl = 0.902, Peak = 0.092

Figure 3-12. Point-spread function for point object 1. The quantities λ and F are the optical wavelength and system focal ratio ($f/\#$).



Aberrated

Corrected

$\sigma_w = 1.06$, Strehl = 0.0038, Peak = 0.064 $\sigma_w = 0.058$, Strehl = 0.896, Peak = 0.896

Figure 3-13. Point-spread function for point object 2.

1. Mirror deformations will not be produced by the actuators used for correction, because, in practice, a mirror is not deformed by the movement of actuators.
2. Some static aberrations will be added to the optical system to simulate a nondiffraction-limited undeformed system.
3. The on-axis wavefront error data may not be provided, since the wavefront sensor placed around the HALO focal plane can not sense it.
4. The actuator influence functions used for mirror figure correction will be slightly different from those used by Itek in their algorithm, to simulate errors in the knowledge of influence function.
5. The influence function for edge actuators may be different from that for interior actuators.
6. A segmented mirror will be used.
7. The mirror size will be approximately the same as the illuminated region.

References

1. V.N. Mahajan, J. Govignon, and R.J. Morgan, "Adaptive Optics Without Wavefront Sensors," Proc. SPIE 228 63-69 (1980).
2. V.N. Mahajan, "ACOSS Eleven Second Semiannual Technical Report, Volume 1," CSDL-R-1583, August 1982.
3. V.N. Mahajan and J. Govignon, "Computer Simulation of a Large Adaptive Optical System," Proc. SPIE 172 439-451 (1979).

DISTRIBUTION LIST

addresses

number
of copiesRichard Carman
RADC/DCSE

5

RADC/TSTD
GRIFFISS AFB NY 13441

1

RADC/DAP
GRIFFISS AFB NY 13441

2

ADMINISTRATOR
DEF TECH INF CTR
ATTN: DTIC-DDA
CAMERDN STA BG 5
ALEXANDRIA VA 22314

12

Charles Stark Draper Lab
555 Technology Square
Cambridge, MA 02139

5

Charles Stark Draper Lab
Attn: Dr. Keto Soosaar
555 Technology Square
M.S. -95
Cambridge, MA 02139

1

NSA Headquarters
ATTN: Mr. J. B. Dahlgren
Code RTH-6
Washington, DC 20546

1

Charles Stark Draper Lab
Attn: Mr. R. Strunce
555 Technology Square
M.S. -60
Cambridge, MA 02139

1

Charles Stark Draper Lab
Attn: Dr. Daniel R. Hegg
555 Technology Square
M.S. -60
Cambridge, MA 02139

1

ARPA/STO 1
Attn: Lt Col A. Herzberg
1400 Wilson Blvd
Arlington, VA 22209

ARPA/STO 1
Attn: Maj E. Dietz
1400 Wilson Blvd
Arlington, VA 22209

Riverside Research Institute 2
Attn. Mr. A. DeVilliers
1701 N. Ft. Myer Drive, Suite 711
Arlington, VA 22209

Riverside Research 1
Attn: HALO Library, Mr. Bob Passut
1701 N. Ft. Myer Drive
Arlington, VA 22209

Itek Corp 1
Attn: Mr Edward Gallet
Optical Sciences Division
10 Maquire Road
Lexington, MA 02173

Perkin Elmer Corp 1
Attn: Mr. H. Levenstein
Electro Optical Division
Main Avenue
Norwalk, CT 06856

Hughes Aircraft Company 1
Attn: Mr. George Speak
W S. B_156
Culver City, CA 09230

Hughes Aircraft Company 1
Attn: Mr. Ken Beale
Sentinela Teale Sts
Culver City, CA 90230

Air Force Flight Dynamics Lab 1
Attn: Dr. Lynn Rogers
Wright Patterson AFB, OH 45433

AFWL/FIBG

1

Attn: Mr. Jerome Pearson
Wright Patterson AFB, OH 45433

Air Force Wright Aero Lab. FIGC
Attn: Siva S. Banda
Wright Patterson AFB, OH 45433

1

Air Force Institute of Technology
Attn: Prof. R. Calico/ENY
Wright Patterson AFB OH 45433

1

Aerospace Corp.
Attn: Dr. G.T. Tseng
2350 E. El Segundo Blvd
El Segundo, CA 90245

2

Aerospace Corp.
Attn: Mr. J. Mosich
2350 E. El Segundo Blvd
El Segundo, CA 90245

1

Aerospace Corp/Bldg 125/1054
Attn: Mr. Steve Burrin
Advanced Systems Tech Div.
2400 E El Segundo Blvd
El Segundo, CA 90245

1

SD/SD/YLVS
Attn: Mr. Lawrence Weeks
P O Box 92960
Worldway Postal Center
Los Angeles CA 90009

1

SD/YCD
Attn: YCPT/Capt Gajewski
P O Box 92960
Worldway Postal Center
Los Angeles, CA 90009

1

Grumman Aerospace Corp
Attn: Dr. A. Mendelson
South Oyster Bay Road
Great Neck, NY 11714

1

JUSDR&E/DS
Attn. Mr. A. Bertapelli
Room 3D136
Pentagon, Washington, DC 20301

1

Jet Propulsion Laboratory
Dr. S. Szermay
4800 Oak Grove Drive
Pasadena, CA 91103

2

MIT/Lincoln Laboratory
Attn: S. Wright
P.O. Box 73
Lexington, MA 02173

1

MIT/Lincoln Laboratory
Attn: Dr. N. Smith
P.O. Box 73
Lexington, MA 02173

1

Control Dynamics Co.
Attn: Dr. Sherman Seltzer
Suite 1414 Executive Plaza
555 Sparkman Drive
Huntsville, AL 35805

1

Lockheed Space Missile Corp.
Attn: A. A. Woods, Jr., D/62-E6
P.O. Box 504
Sunnyvale, California 94088-3504

5

Lockheed Missiles Space Co.
Attn: Mr. Paul Williamson
3251 Hanover St.
Palo Alto, CA 94304

1

General Dynamics
Attn: Ray Halstenberg
Convair Division
5001 Keary Villa Rd
San Diego, CA 92123

1

STI
Attn: Mr. R.C. Stroud
20045 Stevens Creek Blvd.
Folsom, CA 95014

1

NASA Langley Research Ctr Attn: Dr. Earle K. Huckins III Dr. M. F. Card Langley Station, Bldg 1293B, MS 230 Hampton, VA 23665	2
NASA Johnson Space Center Attn: Robert Piland Ms. EA Houston, TX 77058	1
McDonald Douglas Corp Attn: Mr. Read Johnson Douglas Missile Space Systems Div 5301 Bulsa Ave Huntington Beach, CA 92607	1
Integrated Systems Inc. Attn: Dr. N. K. Gupta and M. G. Lyons 151 University Avenue, Suite 400 Palo Alto, California 94301	2
Boeing Aerospace Company Attn: Mr. Leo Cline P.O. Box 3999 Seattle, WA 98124 MS 8 W-23	1
TRW Defense Space Sys Group Inc. Attn: Ralph Iwens Bldg 82/2054 One Space Park Redondo Beach, CA 90278	1
TRW Attn: Mr. Len Pincus Bldg R-5, Room 2031 Redondo Beach, CA 90278	1
Department of the NAVY Attn: Dr. K. T. Alfried Naval Research Laboratory Code 7920 Washington, DC 20375	1
Research Manuf. Co. of Calif. Attn: Mr. Oscar Buchmann 2325 West 190th St. Torrance, CA 90509	1

Analytic Decisions, Inc.
Attn: Mr. Gary Glaser
1401 Wilson Blv.
Arlington, VA 22209

1

Ford Aerospace & Communications Corp.
Drs. I. P. Leliakov and P. Barba, MS/G80
3939 Fabian way
Palo Alto, California 94304

1

Center for Analysis
Mr. James Justice
13 Corporate Plaza
Newport Beach, CA 92660

1

W. J. Schafer Associates
Dr. R. Kappesser
Suite 800
1901 Fort Meyer Drive
Arlington, VA 22209

1

General Research Corp
Attn: Mr. Thomas Zakrzewski
7655 Old Springhouse Road
McLean, VA 22101

1

Air Force Weapons Laboratory
Attn: Capt Terry Hinnerichs
ARAA
Kirtland AFB, NM 87117

2

Farman Sciences Corp.
Attn: Dr. Walter E. Ware
1500 Garden of the Gods Road
P.O. Box 7463
Colorado Springs, CO 80933

1

MRJ, Inc.
10400 Eaton Place
Suite 300
Fairfax, VA 22030

1

Photon Research Associates
Mr. James Myer
P.O. Box 1318
La Jolla, CA 92038

1

Rockwell International
Attn: Russell Loftman (Space Systems Group)
(Mail Code - SL56)
12214 Lakewood Blvd.
Downey, CA 90241

1

Science Applications, Inc.
Attn: Mr. Richard Ryan
3 Preston Court
Bedford, MA 01730

1

U. S. Army Missile Command
Attn: DRSMI-RAS/Mr. Fred Haak
Redstone Arsenal, AL

1

Naval Electronic Systems Command
Attn: Mr. Charles Good
PME_106-4
National Center I
Washington, DC 20360

1

Lockheed Palo Alto Research Laboratory
Attn: Dr. J. N. Aubrun, O/52-56
3251 Hanover Street
Palo Alto, California 94304-1187

2

U. S. Army/DARCOM
Attn: Mr. Bernie Chasnov
AMC Bldg
5001 Eisenhower Ave
Alexandria, VA 22333

1

Defense Documentation Center
Cameron Station
Alexandria, VA 22314

1

Honeywell Inc.
Attn: Dr. Thomas B. Cunningham
Attn: Dr. Michael F. Barrett
3600 Ridgway Parkway MN 17-2375
Minneapolis, MN 55413

2

NASA Marshal Space Flight Center
Attn: Dr. J. C. Blair, ED01
Henry B. Waites
Marshal Space Flight Center, AL 35812

2

TRW
Attn: Robert Benhabib
Bldg 82/2024
One Space Park
Redondo Beach, CA 90278

1

NASA Langley Research Center
Attn: Dr. L. Pinson
MS - 230
Hampton, VA 23665

1

H. R. Textron
Attn. Mr. Richard Quartararo
2485 McCabe Way
Irvine, CA 92714

1

Naval Research Lab
Attn: W. Bennett
Mail Code: 7926
Washington, DC 20375

1

TOTAL COPIES REQUIRED

100

Engineer/LCN Signature

Richard M. Carman 21 Oct 83



MISSION of Rome Air Development Center

RADC plans and executes research, development, test and selected acquisition programs in support of Command, Control Communications and Intelligence (C³I) activities. Technical and engineering support within areas of technical competence is provided to ESD Program Offices (POs) and other ESD elements. The principal technical mission areas are communications, electromagnetic guidance and control, surveillance of ground and aerospace objects, intelligence data collection and handling, information system technology, ionospheric propagation, solid state sciences, microwave physics and electronic reliability, maintainability and compatibility.